GLOBAL BIOGEOCHEMICAL CYCLES, VOL. 11, NO. 3, PAGES 367-392, SEPTEMBER 1997

Interannual variation in global-scale net primary production: Testing model estimates

Carolyn M. Malmström,[1,2,3] Matthew V. Thompson,[1,2,4] Glenn P. Juday,[5]
Sietse O. Los,[6] James T. Randerson,[1,2] and Christopher B. Field[1]

Abstract. Testing estimates of year-to-year variation in global net primary production (NPP) poses some challenges. Large-scale, multiyear records of production are not readily available for natural systems but are for agricultural systems. We use records of agricultural yields at selected sites to test NPP estimates produced by CASA, a global-scale production model driven by both meteorological data and the satellite-derived normalized difference vegetation index (NDVI). We also test estimates produced by the Miami model, which has underlain several analyses of biosphere response to interannual changes in climate. In addition, we test estimates against tree ring data for one boreal site for which data from both coniferous and deciduous species were available. The agricultural tests demonstrate that CASA can reasonably estimate interannual variation in production. The Miami model estimates variation more poorly. However, differences in NDVI-processing algorithms substantially affect CASA's estimates of interannual variation. Of the four versions tested, the FASIR NDVI most closely reproduced yield data and showed the least correlation with changes in equatorial crossing time of the National Oceanic and Atmospheric Administration satellites. One issue raised is the source of the positive trends evident in CASA's NDVI-based estimates of global NPP. The existence of these trends is consistent with potential stimulation of terrestrial production by factors such as CO_2 enrichment, N fertilization, or temperature warming, but the magnitude of the global trends seen is significantly greater than suggested by constraints imposed by atmospheric fluxes.

1. Introduction

The recent development of multiyear sets of satellite and weather data permits modelled estimates of year-to-year variation in global-scale terrestrial production. Estimates based on weather data [*Dai and Fung*, 1993; *Kindermann et al.*, 1996] and on satellite-based measures of vegetation canopy characteristics [*Maisongrande et al.*, 1995; *Myneni et al.*, 1995] have yielded different patterns of interannual variation.

In this paper, we examine estimates of net primary production for 1982-1990, a period with useful satellite data. During this period, significant variation in environmental drivers of production occurred. Atmospheric CO_2 levels measured at Mauna Loa Observatory rose 3.8%, continuing the well-documented upward trend (Figure 1). Mean precipitation on ice-free land fluctuated from ~815 to 846 mm per year, and mean terrestrial temperature rose from about 14.4°C in 1982 to 15.0°C in 1990 (Figure 1). El Niño-Southern Oscillation (ENSO) warm events occurred in 1982-1983 and 1986-1987 (Figure 1), marked by slightly warmer and drier conditions on average, but with strong regional differences [*Trenberth et al.*, 1988; *Trenberth*, 1991; *Lau and Sheu*, 1991].

In assessing variation in production, models that use satellite-based vegetation indices possess an advantage over those that do not. Vegetation indices provide information about the integrated response of plant canopies to environmental factors, including factors that might otherwise be omitted from model algorithms, such as land-use change, CO_2 and N fertilization, irrigation, fire, and defoliation by pests and pathogens. The disadvantage of relying on satellite-based indices is that the raw data reflect variation not only in vegetation canopies but also in satellite and instrument performance, in atmospheric properties, and in reflectance geometry. Raw data must be processed to remove these extraneous signals. However, theories about the best way to apply corrections vary. Consequently, different approaches may be taken, resulting in the production of several different versions of data sets collected by the same instruments. This is the case for the global time series of advanced very high resolution radiometer (AVHRR) data available for the 1980s from the National Oceanic and Atmospheric Administratin (NOAA) polar-orbiting satellites, for which more than four different versions exist [*Goward et al.*, 1994; *James and Kalluri*, 1994; *Los et al.*, 1994; *Ruimy et al.*, 1994; *Townshend*, 1994; *Sellers et al.*, 1996; S.O. Los, manuscript in preparation, 1997].

[1]Carnegie Institution of Washington, Department of Plant Biology, Stanford, California.
[2]Department of Biological Sciences, Stanford University, Stanford, California.
[3]Now at Department of Integrative Biology, University of California, Berkeley.
[4]Now at Department of Organismic and Evolutionary Biology, Harvard University, Cambridge, Massachusetts.
[5]Forest Sciences Department, University of Alaska-Fairbanks, Fairbanks, Alaska.
[6]Science Systems and Applications, Inc., Greenbelt, Maryland.

Paper number 97GB01419.
0886-6236/97/97GB-01419 $12.00

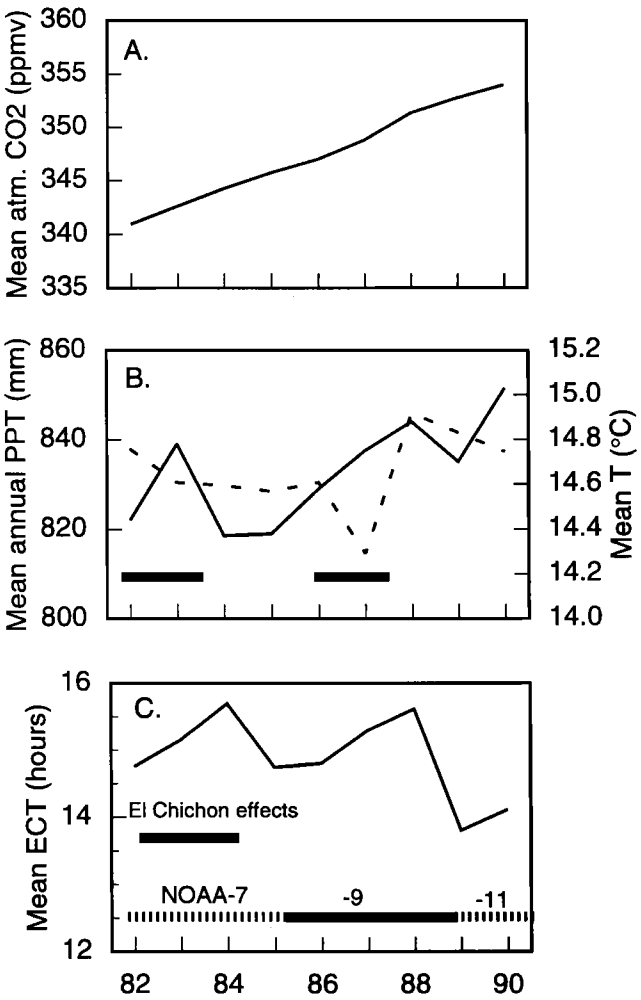

Figure 1. Potential causes of biological and artifactual variation in NDVI time series. (a) Mean annual atmospheric CO_2 levels measured at the Mauna Loa Observatory, from *Keeling and Whorf* [1991]. (b) Mean annual precipitation (dashed line) and mean annual temperature (solid line) for ice-free surfaces from global input sets used to drive the CASA and Miami model runs (see Methods). Precipitation is sum of *Baker et al.* [1995] anomalies and *Shea* [1986] means. Temperature is sum of *Hansen and Lebedeff* [1987, 1988] anomalies and *Shea* [1986] means. Heavy lines indicate ENSO periods. (c) Mean annual equatorial crossing time (see Methods) and time periods for El Chichón effects and NOAA satellites.

Because of the global coverage and short revisit interval, the AVHRR time series are attractive for evaluating dynamics of the terrestrial biosphere. For use in production models, AVHRR data are commonly converted into the normalized difference vegetation index (NDVI), which is the difference between the near-infrared and visible reflectances divided by their sum and which reflects the fraction of light absorbed by vegetation [*Sellers et al.*, 1992]. AVHRR time series of NDVI are sensitive to several nonbiological factors that may introduce artifactual interannual variation. These factors include the following: (1) Temporal and spatial heterogeneity of atmospheric absorption and scattering: The eruption of El Chichón in 1982, for example, produced aerosols that increased atmospheric thickness in the low and midlatitudes until the beginning of 1984, reducing NDVI [*Vermote et al.*, 1994] (Figure 1). Variation in atmospheric water vapor content can be a significant source of seasonal variation in NDVI and may also contribute to interannual variation [*Justice et al.*, 1991]; (2) Satellite switches: NOAA 7 was launched June 23, 1981, NOAA 9 was launched December 12, 1984, and NOAA 11 was launched September 24, 1988 [*Goward et al.*, 1994]. The sensors on the different satellites must be intercalibrated (Figure 1); (3) Sensor degradation: Channels 1 (visible) and 2 (near infrared) degrade at different rates, altering NDVI over time; (4) Changes in equatorial crossing time: The three NOAA afternoon satellites have each slowly fallen behind the Sun's effective rate of progression, with the result that the overpass time of each satellite becomes later as the satellite ages [*Price*, 1991] (Figure 1). Changes in overpass time alter the relationship between Sun angle, view angle, and vegetation, and can alter NDVI estimates [*Los et al.*, 1994; *Privette et al*, 1995; *Sellers et al.*, 1996].

The coincidence of climatic, environmental, and satellite changes makes it difficult to separate each of their signals (Figure 1). During the 1982-1983 ENSO, for example, aerosols from El Chichón increased atmospheric optical depth, and NOAA 7 was drifting notably late. During the 1986-1987 ENSO, NOAA 9 was drifting late; in the La Niña year of 1988, when drought hit the United States and Canada, NOAA 9 was switched with NOAA 11.

How can we test multiyear estimates of global-scale production? For NDVI-based models, how can we test the effects of using different NDVI versions? One approach for testing multiyear estimates of production is to compare the estimates with others derived from deconvolutions of the atmospheric carbon dioxide record [e.g., *Kindermann et al.*, 1996]. In this approach, atmospheric data and estimates of fossil fuel emission, oceanic carbon exchange, and/or land use change are used to infer the pattern of net carbon uptake (net ecosystem production) (NEP) by terrestrial systems over a given period [*Houghton*, 1993; *Francey et al.*, 1995; *Keeling et al.*, 1995; *Sarmiento et al.*, 1995]. Since net carbon uptake is the sum of the carbon taken up in net primary production (NPP) and the carbon released in heterotrophic respiration, estimates of production may be added to estimates of heterotrophic respiration and compared with the inferred values of NEP. One disadvantage of this approach is the need to rely on numerous models beyond the production model being tested. Another limitation is that there is some disagreement between the estimates of NEP produced todate [*Houghton*, 1993; *Francey et al.*, 1995; *Keeling et al.*, 1995; *Sarmiento et al.*, 1995].

Testing production estimates against production data directly circumvents these limitations. When testing estimates of production for a single year (or estimates of mean production), the approach typically has been to compare grid cell estimates with measurements taken in the field at selected sites in different ecosystems [e.g., *Raich et al*, 1991; *Potter et al.*, 1993]. However, this approach also has its limitations. In natural ecosystems, there are two primary constraints, one related to the temporal scale, the other to the spatial scale. (1) Production data at a given site are generally available only for a single year, which may not necessarily be the same year as that for the other sites or for the model estimate. Such

Table 1. Comparison of Processing of NDVI Versions

Version	Atmospheric and Cloud Corrections	Sensor Calibration and Degradation	Solar Zenith Angle	Additional Features
CESBIO	Rayleigh scattering; in GVI: weekly maximum difference composite of DN	*Kaufman and Holben* [1993]	SZA > 75°, 85° removed[a]; maximum value compositing on difference of DN leads to selection of data from extreme backscatter directions. NDVI values at high SZA are lower than for versions below.	best index slope extraction, *Viovy et al.* [1992]
PRE: global 1 °x 1° GIMMS	El Chichón correction; in GIMMS: channel 5 cloud screening and maximum value compositing	approximation, *Los* [1993]; in GIMMS: preflight calibration	SZA > 85° removed	scan angle cutoff: 42° off-nadir
FASIR 2.1	same as PRE	same as PRE	same as PRE, plus: SZA correction, *Sellers et al.* [1996]; S. O. Los (manuscript in preparation, 1997)	scan angle cutoff: 42° off-nadir; Fourier adjustment; winter value interpolation; tropical reconstruction, *Sellers et al.* 1996]; S. O. Los (manuscript in preparation, 1997)
Pathfinder	Rayleigh scattering[b]; ozone absorption; cloudflagging; maximum value compositing	*Rao* [1993a, b]; *James and Kalluri* [1994]; *Rao and Chen* [1995]	SZA > 80° removed	scan angle cutoff: 42° off-nadir

[a]SZA in CESBIO were screened twice, first at 85°, and then at 75° when atmospheric corrections were applied.
[b]In Pathfinder, corrections for Rayleigh scattering are applied only to incoming radiation.

mismatch of years introduces error into the comparisons. (2) The sites from which the data are collected are typically much smaller than the model grid cells in which they are nested and may not adequately represent them. For example, production measurements made in a small nature reserve may not fairly represent production in the rest of the grid cell, if the area outside the reserve has been degraded by heavy grazing.

Thus developing methods for testing interannual variation in global-scale production presents a two-part problem: How to find (1) time series data that (2) represent large areas? This sort of data is currently not available for natural systems. However, the agricultural sector has been measuring large-scale production patterns for years, and these data are readily available. In forested ecosystems, tree ring data also provide information about interannual growth patterns. Unlike agricultural production data, however, tree ring data is typically small-scale in nature (individual trees are sampled), which makes it more difficult to compare with grid-cell estimates. In this paper, we describe the first attempt to use records of agricultural yields at selected sites to test estimates of interannual variation in net primary production. We also suggest an approach for extrapolating tree ring data to test estimates in forested systems.

In this analysis, we examine regional and global estimates produced by two models: (1) the Miami model [*Lieth*, 1975], which is driven solely by meteorological data, and which has underlain many analyses of biosphere response to interannual changes in climate, including recent studies by *Dai and Fung* [1993]; and *Friedlingstein et al.* [1995]; (2) The Carnegie-Ames-Stanford-Approach Biosphere Model (CASA)[*Potter et al.*, 1993; *Field et al*, 1995], a light-use efficiency model driven by both meteorological and NDVI data.

We also compare the effects of driving CASA with four different 1° x 1° versions of monthly NDVI (see Methods, Table 1, and Figure 2 for more detailed descriptions): (1) CESBIO NDVI produced by the Centre d'Etudes Spatiales de la Biosphère (France) [*Ruimy et al.*, 1994]; (2) a 1° global version of the 5-8 km data processed by the Global Inventory Monitoring and Modelling Studies (GIMMS) group at NASA Goddard Space Flight Center (U.S.A.), which we refer to as "PRE" [*Los et al.*, 1994]; (3) FASIR 2.1, a version of PRE (above) to which the following additional corrections have been applied: Fourier adjustment, solar zenith angle correction, interpolation of high-latitude winter values, and reconstruction of values over tropical regions [*Sellers et al.*, 1996; S. O. Los, manuscript in preparation, 1997]; (4) Pathfinder NDVI produced by the NOAA/NASA Pathfinder program (U.S.A.) [*James and Kalluri*, 1994; *Townshend*, 1994].

2. Methods

2.1. Models

The Miami model [*Lieth*, 1975] is one of the original models of net primary production. It is a simple empirical

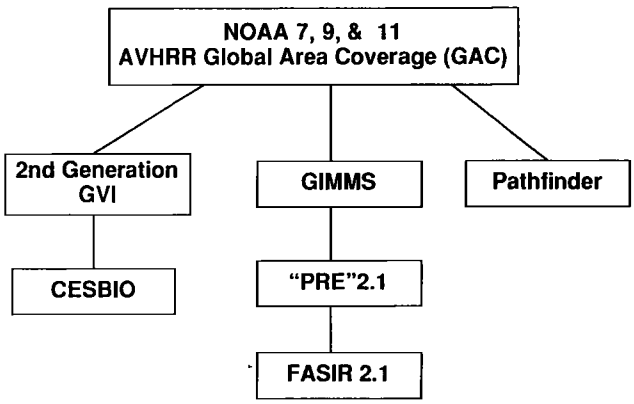

Figure 2. Family tree of monthly 1° x 1° NDVI versions discussed in this paper. The CESBIO version [*Ruimy et al.*, 1994] was produced by the Centre d'Etudes Spatiales de la Biosphère (France) from the weekly second generation Global Vegetation Index (GVI) product [*Tarpley et al,* 1984]. "PRE" is a maximum-value composite produced by *Los et al.* [1994] from the 5-8 km data processed and archived by the Global Inventory Monitoring and Modelling Studies (GIMMS) group at NASA Goddard Space Flight Center (U.S.A.). FASIR 2.1 is the result of applying additional corrections to "PRE": a Fourier adjustment, solar zenith angle correction, winter value interpolation, and tropical reconstruction [*Sellers et al,* 1996; S.O. Los, manuscript in preparation, 1997]. Pathfinder is a reprocessing of the AVHRR GAC data, produced as a NASA/NOAA contribution to the Earth Observing Systems program (U.S.A.) [*Agbu and James*, 1994; *James and Kalluri*, 1994]. CESBIO, PRE, FASIR, and Pathfinder have all been adjusted to account for sensor degradation, but the degree of cloud screening and atmospheric corrections varies across versions. Only FASIR has been explicitly adjusted for variation in solar zenith angle. For more detailed descriptions of the versions, see Methods and Table 1.

model that calculates NPP (g dry matter $m^{-2} yr^{-1}$) on an annual time step as a function of annual temperature and annual precipitation.

$$NPP = \min \{ (3000)/[1.0 + \exp(1.315 - 0.119 \times airT] \quad 3000\,(1.0 - \exp(-0.000664 \times PPT)) \} \qquad (1)$$

where airT is mean annual temperature in degrees Celsius and PPT is total annual precipitation in mm yr^{-1}. Outside of tundra, boreal forest, and cold desert ecosystems, NPP is generally determined by the PPT limitation. The Miami model was originally conceived as a tool for estimating the spatial distribution of NPP, based on long-term climate means. However, it has recently been used to examine patterns of year-to-year variation in NPP as well [e.g., *Dai and Fung,* 1993; *Friedlingstein et al.*, 1995], and we include it here for this reason.

The CASA model is a global-scale model that uses both meteorological data and NDVI to estimate monthly carbon fluxes within and from the terrestrial biosphere, for 1° x 1° grid cells [*Potter et al.*, 1993; *Field et al.*, 1995; *Malmström et al.*, 1995; *Thompson et al.*, 1996; *Randerson et al.*, 1996]. Net primary production is estimated from intercepted radiation and light use efficiency [*Monteith,* 1972, 1977]:

$$NPP(x,t) = IPAR(x,t)\,\varepsilon(x,t) \qquad (2)$$

where IPAR (x,t) is intercepted photosynthetically active radiation (MJ m^{-2} $month^{-1}$) and ε(x,t) is light-use efficiency (g C MJ^{-1} PAR).

$$IPAR(x,t) = \text{solar radiation}\,(x,t) \times 0.5 \times FPAR\,(x,t) \qquad (3)$$

where solar radiation (total surface solar irradiance) is multiplied by 0.5 to approximate MJ PAR [*Nobel*, 1991]. FPAR (x,t) is derived by the method of *Sellers et al.* [1996] from simple ratio (SR), a transformation of NDVI that has been shown to be approximately linearly related to FPAR

$$SR = (1+NDVI)/(1-NDVI) \qquad (4)$$

The FPAR function is scaled as a function of vegetation type as

$$FPAR = \frac{(SR - SR_{i,min})(FPAR_{max} - FPAR_{min})}{(SR_{i,max} - SR_{i,min})} + FPAR_{min} \qquad (5)$$

where $FPAR_{max}$ = 0.950 and $FPAR_{min}$ = 0.001, independent of vegetation type, $SR_{i,max}$ = SR value corresponding to the 98th percentile of NDVI population i, and $SR_{i,min}$ = SR value corresponding to the 5th percentile of NDVI population i. For each NDVI version we used, we calculated the 98th and 5th percentiles of the NDVI populations for the different vegetation types and used equations (4) and (5) to scale the FPAR to NDVI relationship. Light use efficiency is calculated as

$$\varepsilon(x,t) = \varepsilon^* T_1(x,t)\, T_2(x)\, W(x,t) \qquad (6)$$

ε* is the global maximum light use efficiency in g C MJ^{-1}, T_1 and T_2 are scalars that represent temperature constraints on productivity, and W is a scalar that describes the effects of soil moisture availability. T_1 reduces ε when mean air temperature is less than or greater than an optimum temperature, defined for each grid cell as T_{opt}, the temperature during the month of maximum NDVI. T_2 reduces ε to the degree that T_{opt} departs from 20°C, to reflect the incomplete nature of physiological compensation for non-optimal temperatures [*Field et al.*, 1995]. W, the soil moisture constraint, is a nonlinear function of soil moisture, based on a one-layer bucket model with a nonlinear drying factor.

For each model run, ε* is determined by a least squares fit of observed NPP values at sites in 71 grid cells against CASA's NPP estimates for the same cells [*Potter et al.*, 1993; *Field et al.*, 1995]. ε* ranged from 0.489 g C MJ^{-1} PAR for CASA run with variable FASIR NDVI to 0.651 g C MJ^{-1} PAR with variable CESBIO NDVI.

2.2. Global Input Sets for CASA and Miami Runs

The CASA runs used the data sets as described below. The Miami model runs used annually aggregated precipitation and temperature.

2.2.1. Climatological data. Monthly precipitation anomaly data with 5° x 5° resolution for 1982-1990 from *Baker et al.* [1995] were rebinned to 1° x 1°. These anomalies were added to monthly mean values from 1950-1979 [*Shea*, 1986], also gridded to 1° x 1°, to obtain total monthly values for the 1982-1990 period. Although the Shea set has less orographic detail than the *Leemans and Cramer* [1991] set, the

Shea means originate from the same period as those used to derive the Baker et al. anomalies and thus are a better complement. Nonetheless, the sum resulted in some negative values in dry regions, which were truncated to zero. Monthly air surface temperature anomaly data for 1982-1990 were from a continuously updated anomaly set [*Hansen and Lebedeff*, 1987, 1988], rebinned to 1° x 1°, and added to monthly means from 1950-1979 [*Shea*, 1986]. Mean monthly surface solar irradiance values for July 1983 to December 1990 were from *Bishop and Rossow* [1991]. For January 1982 to June 1983 we substituted the monthly means from 1984 to 1990.

2.2.2. NDVI data. We used four recent versions of monthly 1° x 1° NDVI derived from AVHRR Global Area Coverage (GAC) data from the polar-orbiting TIROS/NOAA 7, 9, and 11 satellites (Table 1, Figure 2). The degree of cloud screening and correction for atmospheric scattering and absorption varies across the versions. All had sensor degradation corrections applied. Only the FASIR version was explicitly corrected for variation in solar zenith angle (SZA); the CESBIO, PRE, and Pathfinder versions simply remove values at extreme solar zenith angle. Note that PRE and FASIR share the same correction for El Chichón aerosols.

1. CESBIO (1986-1991) [*Ruimy et al.*, 1994], produced by the Centre d'Etudes Spatiales de la Biosphère (France), is based on the second generation NOAA/AVHRR weekly GVI product [*Tarpley et al.*, 1984], with additional corrections for Rayleigh scattering, sensor calibration, and data discontinuity (Table 1). The transition from NOAA 9 to NOAA 11 in November 1988 is visible as a discontinuity in this version, as noted by *Maisongrande et al.* [1995]. The CESBIO version was used in *Maisongrande et al.*'s [1995] analysis of interannual variation in NPP.

2. "PRE" 2.1 (1982-1990) is a 1° x 1° monthly maximum-value composite produced by *Los et al.*. [1994] from the 5-8 km data processed and archived by the Global Inventory Monitoring and Modelling Studies (GIMMS) group at NASA Goddard Space Flight Center. Corrections for the El Chichón eruption and for sensor calibration have been applied (Table 1). The El Chichón correction is described in Appendix C. We refer to this version as "PRE" because it is a precursor to FASIR 2.1 described below.

3. FASIR 2.1 (1982-1990) [*Sellers et al.*, 1996; S.O. Los, manuscript in preparation, 1997] is based on "PRE," with added Fourier adjustment, solar zenith angle correction, winter value interpolation, and tropical reconstruction (Table 1). It is designed for use in climate studies [*Sellers et al.*, 1996]. The FASIR solar zenith angle correction is described in Appendix C.

4. Pathfinder (1982-1992) [*Agbu and James*, 1994; *James and Kalluri*, 1994; *Townshend*, 1994] represents a reprocessing of the AVHRR GAC data, as a NASA/NOAA contribution to the EOS program. Corrections for Rayleigh scattering (incoming radiation only), ozone absorption, and sensor calibration were applied (Table 1). We used the maximum monthly composite version of this series, available globally at the 1° x 1° scale. The Pathfinder processing used incorrect scan angles and solar zenith angles for some nadir pixels greater than 55°N, but these pixels are generally excluded from the composite because of high scan angle [*Agbu and James*, 1994].

For comparison, annual mean equatorial crossing time (mean solar time) was calculated following *Rosborough et al.* [1994] as recommended by the NASA EOS-DAAC (Figure 1). We used values for NOAA 7 from January 1, 1982, through February 28, 1985; for NOAA 9 from March 1, 1985, through November 17, 1988; and for NOAA 11 from November 18, 1988, through December 31, 1990. These dates correspond to the change of source satellite for the FASIR and PRE products [*Los*, 1993; *Los et al.*, 1994] and are very close to those used by the CESBIO and Pathfinder products.

2.2.3. Other data. For soil texture information we used the *Zobler* [1986] soil texture map. For global vegetation classification we used the 12-class AVHRR-based map produced by *DeFries and Townshend* [1994, 1995].

2.3. Agricultural Data

2.3.1. Selection of sites. The seven test areas selected were the South Australian wheat region, the Saskatchewan Prairie wheat region in Canada, the Moroccan wheat and barley region, the Polish cereal grain region, the Turkish wheat region, and the Kansas and Oklahoma wheat regions in the United States (Table A1). Several selection criteria were employed.

1. The test sites are larger than the 1° x 1° grid cell scale of the model and the NDVI input sets used. Within some limits, larger samples are preferable to smaller ones because there is some georegistration error in the NDVI data (~4-8 km) [*Los et al.*, 1994] and because the precipitation anomaly set used was originally 5° x 5° in scale [*Baker et al.*, 1994]. The number of grid cells contained in the sites selected ranged from 11 to 58.

2. The test sites are dominated by a particular crop or a simple crop mix, with similar agricultural years. This is one of the biggest constraints on site selection. Yields of dissimilar crops from small, patchy fields are difficult to convert to a single production number comparable to 1° x 1° NPP estimates. Much of the agriculture production in the world falls under this description and so was not appropriate for consideration. Doublecropping, intercropping, and complicated rotations also make interpretation difficult, particularly when the different crops have different canopy structures and/or harvest indices.

3. The test sites match geographic units for which consistent, ground-based yield data are available.

4. The test sites contain little irrigated acreage. This was perhaps the second greatest constraint on site selection: irrigated acreage is interwoven into a substantial number of agricultural regions. Because both the CASA model and the Miami model calculate the effects of moisture availability on production as a function of precipitation, not irrigation, the inclusion of significant irrigated acreage would confound the estimates.

The locations of the agricultural regions were determined from the sources listed in Table A2 (see Appendix A for details). These regions were then compared with the satellite-based *DeFries and Townshend* [1995] vegetation classification, and grid cells not categorized as Class 12 (agriculture) were removed. In the test regions the DeFries and Townshend classification was typically more conservative (classified less area as agriculture) than ground-based maps.

2.3.2. Agricultural yields. The sources of yield data are described in Appendix A. At some sites, growing seasons overlap 2 calendar years. Winter wheat in Kansas, for example, is planted in September and harvested in June/July of the following year [*Smika*, 1992]. Thus annual NPP estimates refer to the period between January and December for South Australia and Canada, where the crop cycle is contained within 1 calendar year, and between September and August for the other five sites, where crops remain in the ground over the winter. For the latter sites the year beginning September 1982 and ending August 1983, for example, is referred to as 1983. Because of data limitations, the September-August series contain 1 less year than the January-December series.

2.4. Tree Ring Data

2.4.1. Site selection. In forested systems one source of information about interannual variation in production is tree ring data. Traditional dendrochronology has focused on evaluating the growth patterns of individual trees selected for their sensitivity to a particular climate factor, such as summer temperature. This is an effective approach for developing proxy time series of climate variables [e.g., *Briffa et al.*, 1995; *Jacoby and D'Arrigo*, 1995, 1989]. Here, however, the goal is a different one: to develop a tree ring index that captures the interannual growth patterns of an entire 1° x 1° forested grid cell and the forest's response to the full suite of ecological variables, not just to one. The challenge is to find tree ring data that fairly represents the growth patterns of a stand of that size, taking into account the mix of species, the age class distribution, and the nature of growth in a closed canopy. Thus we looked for tree ring data for which there were available: (1) stand-level measurements from large areas of closed canopy forests, (2) data representing the different dominant species, particularly those that differ in sensitivity to environmental factors, and (3) information about the areal extent of forest species, for extrapolating to the grid cell scale.

We include in our tests one site for which we found such data, in the boreal forest at Fort Richardson, Alaska, U.S.A. (Appendix B). Although limited in scope, we include the tree ring comparison because it demonstrates a technique worth further development. If additional data sets are developed, this approach could help refine estimates of year-to-year variation in production in nonagricultural systems.

2.4.2. Different climate sensitivities of dominant forest species. An important aspect of the Fort Richardson data is that stand-level measurements of the two dominant species (spruce and birch) were available (Appendix B). Because these two dominants show different sensitivity to climate variables, an estimate of forest-level production needs to be based on measurements from both. The ring width time series for the two species are notably different for the 1980s (Figure B1). Long-term analysis of ring width response to climate variables in this area indicates that birch growth is positively correlated with precipitation patterns and negatively correlated with temperature, while spruce growth is positively correlated with temperature (G. P. Juday and S. A. Marler, manuscript in preparation, 1997). For the 1980s the birch ring pattern is also more dynamic than the spruce pattern, probably because of the greater sensitivity of birch to short-term growing conditions. In contrast, the growth of spruce in a given year is highly correlated with growth in previous years. This is in part because the needles of the spruce canopy are long-lived. In spruce, several years of strong growth will result in a well-stocked canopy that buffers the trees somewhat from resource fluctuations for the next few years, although sudden events like snow breakage or defoliation by insects can sharply affect growth. The buffering effect may explain why spruce ring widths at this site do not decrease for 1985-1987 in the same way as the birch ring widths do (Figure B1). The period 1979-1981 was the warmest on record for the area (instrument records date from 1934) and resulted in strong spruce growth at this site with likely carryover to subsequent years (G. P. Juday and S. A. Marler, manuscript in preparation, 1997).

2.4.3. Scaling to the grid cell. The measurements were taken from stands within a portion of a single 1° x 1° grid cell (centered on 61.5°N, 149.5°W) comprised primarily of boreal forest. To permit comparison of the ring measurements with estimates of variation in NPP at the 1° x 1° scale, we used a land cover classification based on Landsat Thematic Mapper data [*U.S. Geological Survey*, 1994] to calculate how much area within the grid cell was covered by coniferous forest (primarily spruce), by deciduous forest (primarily birch), and by mixed forest. We assumed that mixed forest was 50% coniferous and 50% deciduous. To estimate a mean ring width for the entire grid cell, we averaged the ring widths of the spruce and birch, weighting them by the area of coniferous and deciduous forests.

$$RW_{\text{grid cell}} = \frac{[RW_{sp}(A_c + 0.5A_m)] + [RW_{bir}(A_d + 0.5A_m)]}{A_c + A_d + A_m} \quad (7)$$

where $RW_{\text{grid cell}}$ is the estimated mean ring width for the grid cell, RW_{sp} is the spruce ring width, RW_{bir} is the birch ring width, A_c is the area covered by coniferous forest, A_d is the area covered by deciduous forest, and A_m is the area covered by mixed forest. This approach resulted in weighting the ring widths as 1 spruce to 1.2 birch.

Because of the difference in growth of spruce and birch, it was not surprising that most of the variation in this average was due to the birch contribution (Figure B1) and that the NDVI-based NPP estimates more strongly correspond to variation in birch growth than in spruce growth (Table B1). The weighted average, however, predicts NPP estimates somewhat better than the birch data alone.

2.5. Analytical Strategy

To evaluate the effectiveness of different models and NDVI versions in capturing interannual variation in production, we tested NPP estimates against agricultural yield data and tree ring data. We quantified fit by calculating the Pearson product-moment correlation coefficient (R) for the data and model estimates at each site. The correlation coefficient is a useful index, but visual inspection of the data yields additional information about the pattern of fit. We therefore also inspected the entire set of data and looked for patterns of mismatch between the data and the NPP estimates, particularly repeated patterns or patterns correlated with satellite switches and changes in satellite equatorial crossing time. Because

there are only 8-9 points per time series, which limits statistical power, we indicate all P values and refer to pairs of series where $0.05 < P \leq 0.10$ as "somewhat" correlated.

We also evaluated estimates of interannual variation in production by vegetation classes and at the global scale. We compared global-scale estimates with published estimates produced by the Frankfurt Biosphere Model [*Kindermann et al.*, 1996; *Lüdecke et al.*, 1994] and by the *Maisongrande et al.* [1995] model and with estimates derived from deconvolutions of the atmospheric carbon dioxide record [*Thompson et al.*, 1996].

For the comparisons we used the Miami model and the CASA model run in three different modes. The three modes were as follows:

1. In the standard model run, CASA was driven with both variable NDVI and variable climate (precipitation, air temperature, and surface solar irradiance) for the period 1982-1990. For this run we used the FASIR NDVI version.

2. In the CASA climate run, only the climate data varied from year-to-year. The NDVI set was the 9-year mean of FASIR 2.1. This run shows the performance of the CASA climate algorithm. Because the CASA model assumes that capturing the natural variation in NPP requires information from both NDVI and climate variables, the estimates produced by the CASA climate algorithm alone should show less dynamic variation than climate models designed to estimate NPP without NDVI input.

3. In the variable NDVI runs, the NDVI data were variable, but the climate inputs were replaced with 9-year means. These runs allowed direct comparison of the contributions of four different NDVI versions: FASIR, PRE, Pathfinder, and CESBIO. The CESBIO series is shorter, so quantitative comparisons with it are limited.

3. Results and Discussion

3.1. Comparison of Model Estimates With Agricultural and Tree Ring Data

In this section, we examine two questions: (1) Can CASA or the Miami model predict year-to-year variation in agricultural production or in mean radial growth of forest stands? (2) What are the consequences of using different NDVI versions in the CASA model?

3.1.1. Comparison of CASA's mean NPP estimates with mean agricultural yields. We first compare mean yields at each site with mean NPP estimates produced by the standard CASA model run with FASIR NDVI (Table 2). Yields in strongly water-limited regions like South Australia and Morocco are low, whereas those in more temperate regions, like Poland, are higher. The mean NPP estimates from the standard CASA model run with FASIR NDVI reflect these differences.

Two factors regulate the relationship between NPP and yield: the aboveground fraction of NPP, and harvest index (the amount of grain produced per unit of aboveground biomass of crop [*Hay*, 1995]). Both factors vary, regionally and temporally. If harvested grain has a 10% moisture content [*Mattern*, 1991] and plant biomass is on average 45% carbon [*Schlesinger*, 1991], and if harvest index (HI) and the aboveground fraction of NPP (AF) are known, yield can be estimated from NPP as

$$Yield_{est} = (NPP_{est} \times AF \times HI)/[0.90 \times 0.45] \quad (8)$$

where $Yield_{est}$ is in g grain m^{-2} and NPP_{est} is in g C m^{-2}.

Because of large uncertainties about belowground production, estimates of the aboveground fraction of NPP (AF) are poorly constrained, ranging from 0.50 to above 0.71 [*Siddique et al.*, 1990]. The range for harvest index for each site is better understood because field measurements are available (Table 2). CASA's NPP estimates can be converted into yield estimates by stipulating values of AF and HI (equation (8)). We calculated low-end yield estimates by setting AF = 0.50 and HI to the low end of the observed values. Similarly, we calculated high-end estimates by setting AF=0.71 and HI to the high end of the observed values. The range of yield estimates can be compared with actual yield values (Table 2). The yield estimates bracket the actual yield values in all cases, except South Australia, where the actual yield is within 3% of the low-end estimate. Yield estimates will be high or low as a function of the accuracy of the estimates of HI, AF, and NPP. Yield estimates will be low, for example, if CASA's NPP estimate is lowered by grid cell heterogeneity in which crop fields are interspersed with less productive areas.

In general, the mean NPP estimates produced by CASA are reasonable. A more constrained test would require separate estimates of belowground and aboveground production, as will be permitted by allocation algorithms under development.

3.1.2. Comparison of patterns of interannual variation. This section examines interannual variation in estimates produced by the standard CASA model and the Miami model, by the climate and NDVI components of the CASA model, and by different NDVI versions.

3.1.2.1. Estimates by standard CASA model and Miami model: The interannual variation in NPP estimated by the standard CASA model run matches yield data at six of the seven agricultural test sites. The model estimates are strongly correlated with yields at four sites (South Australia, Canada, Morocco, and Poland), somewhat correlated ($0.05 < P \leq 0.10$) at two sites (Turkey and Kansas), and not at all correlated in Oklahoma (Figures 3a-3h, top graphs, and Table 3). The lower level of correlation for Turkey and Kansas results primarily from misfit in 1983-1984; for the rest of the period the NPP estimates follow the yield data well. Low yields due to 1982 ENSO-related drought in Australia and the La Niña-related 1988 drought in Canada are evident.

At the boreal forest site the standard CASA estimates are not significantly correlated with radial growth (Figure 4 and Table 4). But this lack of correlation occurs because there is a 4.8% per year trend in the CASA estimates not present in the tree ring data (see "Sources of error," below). When detrended, the CASA estimates are strongly correlated with the tree ring data (Figure 4 and Table 4).

The CASA model describes interannual variation in yield much better than the Miami model. The Miami model's NPP estimates are strongly correlated with yield only in South Australia (Figures 3a-3h, top graphs, and Table 3) and somewhat correlated in Turkey. The Miami estimates are negatively correlated with yield in Oklahoma.

At the boreal forest site the Miami estimates are somewhat anticorrelated with mean tree ring width (Figure 4 and Table 4). This negative correlation likely arises because at this site

Table 2. Comparison of Actual Yields and Estimated Yields Derived from CASA's NPP Estimates (Equation (8)), Mean Values for 1982-1990

	Mean CASA Estimate of NPP, g C m^{-2} yr^{-1}	Measured Harvest Index	Mean Yield, g m^{-2} yr^{-1}	Estimated Mean Yield Based on CASA NPP, Low End, g m^{-2} yr^{-1}	Estimated Mean Yield Based on CASA NPP, High End, g m^{-2} yr^{-1}
South Australia wheat	318.8	0.34-0.38[a]	129.5	133.8	212.4
Canada: Saskatchewan wheat	247.5	0.375-0.412[b]	171.6	114.6	178.8
Morocco wheat and barley	261.4	similar to Australia	116.5	109.7	174.1
Poland total grain	400.7	0.45-0.60[c]	291.7	222.6	421.5
Turkey wheat	272.0	between Australia and U.S.	195.6	107.5	209.8
U.S.: Kansas wheat	412.4	0.31-0.51[d]	240.6	157.8	368.7
U.S.: Oklahoma wheat	400.1	0.31-0.51[d]	212.9	153.1	357.7

Low-end yield estimates assume low-end values of harvest index and aboveground fraction of NPP, high-end yield estimates assume high-end values (see text). Ranges for Morocco and Turkey are estimated based on yields and cultural conditions.

[a]*Siddique et al.* [1989].

[b]*Hucl and Baker* [1987].

[c]*Hay* [1995] says HI values for temperate small-grain cereal crops have reached a plateau in this range. Comparable figures for UK wheat are 0.43-0.54.

[d]*Hay* [1995].

the Miami estimates are determined by annual temperature. The variation in mean tree ring widths, however, is driven largely by the variation in the birch widths, which tend to be correlated negatively with temperature (G.P. Juday and S.A. Marler, manuscript in preparation, 1997).

3.1.2.2. Components of standard CASA model: FASIR NDVI and climate module: The CASA model assumes that capturing the natural variation in NPP requires information from both NDVI and climate variables. The light use efficiency paradigm suggests that vegetation responds to variations in resource availability in two general ways: by altering leaf area index, and thus the fraction of light intercepted, or by altering the efficiency with which light energy is converted to production. In CASA, solar radiation determines the light available at the surface, NDVI provides information about the fraction of light intercepted, and precipitation and temperature regulate light use efficiency. Thus the estimates produced by the standard CASA run combine the effects of climate and NDVI (FASIR 2.1).

The contribution of the climate variables to CASA's multiyear estimates can be seen in runs where NDVI is held constant and climate varies. Conversely, the contribution of the NDVI can be seen when the climate is constant and the NDVI varies (Figures 3a-3h, middle panels). Table 5 shows the semipartial correlation coefficients for the linear regression of FASIR-based estimates and climate-based estimates against standard CASA estimates. These coefficients are approximate indices of the contribution of the different variables to the NPP estimates at each site. For all of the sites, except Canada, the FASIR NDVI contribution dominates the climate contribution. The CASA climate submodule is not directly comparable to the Miami model because it is a submodule designed to describe only one part of the variation in production, that part not captured by changes in NDVI.

The variable FASIR NDVI run generally predicts interannual variation better than the CASA climate run (Figures 3a-3h and Table 3). The FASIR estimates are strongly correlated with yield in five of the seven agricultural sites (South Australia, Morocco, Poland, Turkey, and Kansas), somewhat correlated in Saskatchewan, and, when detrended, strongly correlated with radial growth at the boreal site (Figure 4 and Table 4). In contrast, the CASA climate estimates are correlated with yield only in South Australia and Canada.

When both the CASA climate algorithm and the variable FASIR run correspond fairly well to the yield pattern, the standard CASA run fits the data well (Figures 3a-3h and Table 3). If one component is less accurate, as when the CASA climate algorithm does a poor job for Kansas, Poland, or Turkey (Table 3 and Figure 3), the estimates of the standard run are compromised.

3.1.2.3. Sources of error: At the agricultural sites, mismatches can result from errors in the data sets, weaknesses in the models, natural variance in the NPP-to-yield relationship, changes in cultivation practices, and contamination of the NDVI signal by secondary crops. Since we are most interested in mismatches due to the first two factors, we chose sites to minimize error due to extraneous crop signals. The Saskatchewan wheat region, for example, produces barley as well as wheat. However, the barley fields introduce little mismatch into the estimates because their acreage is smaller and because barley and wheat in this region have similar stature and growing cycles and respond similarly to climatic variation (Figure 5a). Acreage locations were matched to the 1°x1° model grid cells as accurately as possible, but because most of these agricultural regions are relatively large, the results presented are not very sensitive to the exact choice of grid cells. For example, interannual variation in yield is similar for Saskatchewan wheat (31 grid cells) and the larger Canadian prairie region (51 grid cells) that encompasses parts of Alberta and Manitoba as well (Figures 3b and 3c). In choosing sites we also attempted to minimize error due to changes in cultivation practices (e.g., in fertilizer application rates or in cultivars planted). We eliminated our

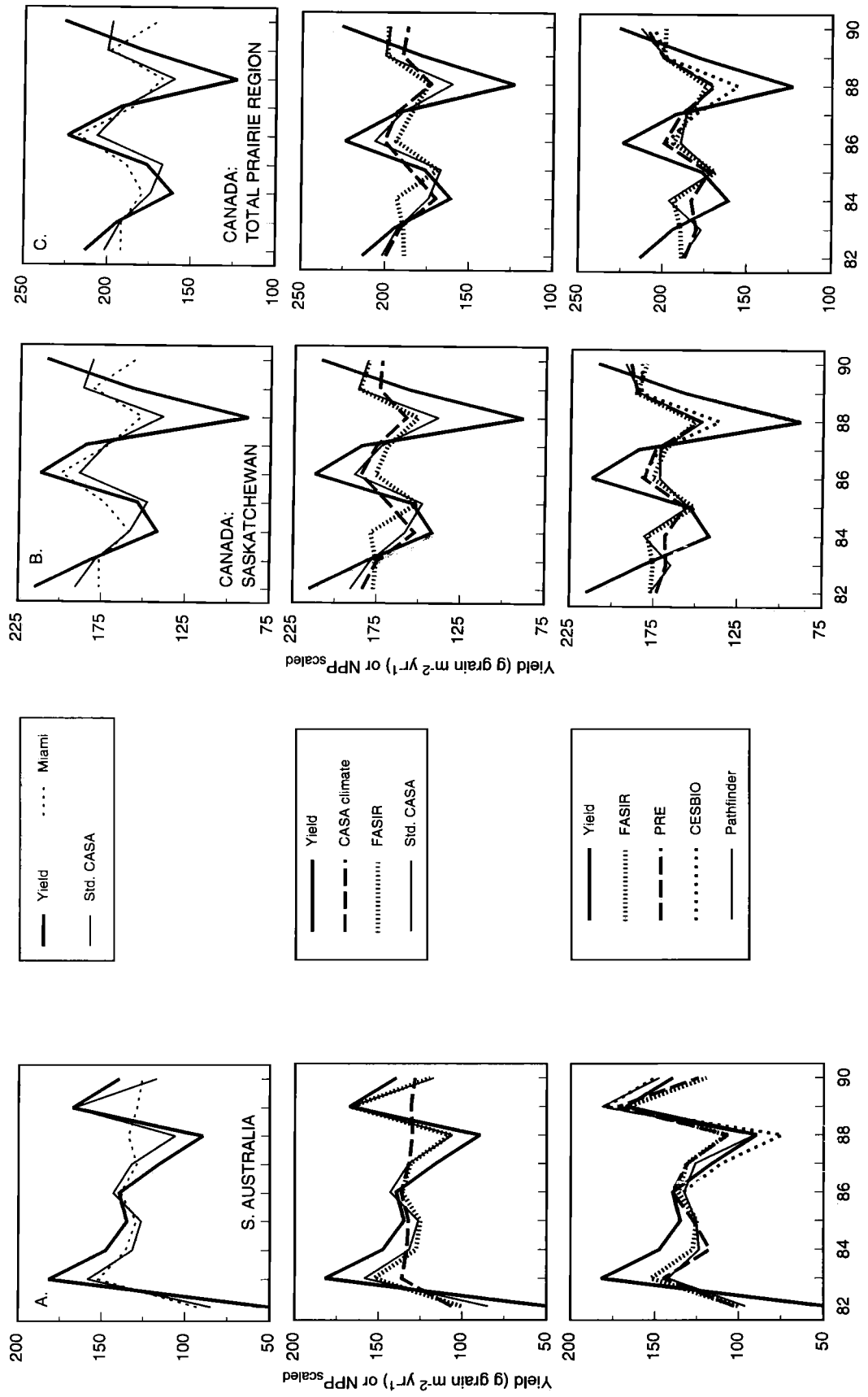

Figure 3. Comparisons of agricultural yield data and NPP estimates. The scales of the graphs are identical, but offset vertically. To make visual comparisons easier, the NPP estimates are scaled to the yield data. For each site, NPP_{scaled} = NPP (mean yield/mean NPP), where the means are the means (1982-1990) at that site. (top panels) Yield data and NPP estimates produced by standard CASA run and the Miami model, scaled by mean to the yield data. (middle panels) Contribution of components of standard CASA run. Yield data and scaled estimates produced by the standard CASA run, variable FASIR NDVI, and the CASA climate algorithm. (bottom panels) Comparison of NDVI versions. Yield data and scaled estimates produced by variable NDVI CASA runs with the FASIR, PRE, Pathfinder, and CESBIO versions.

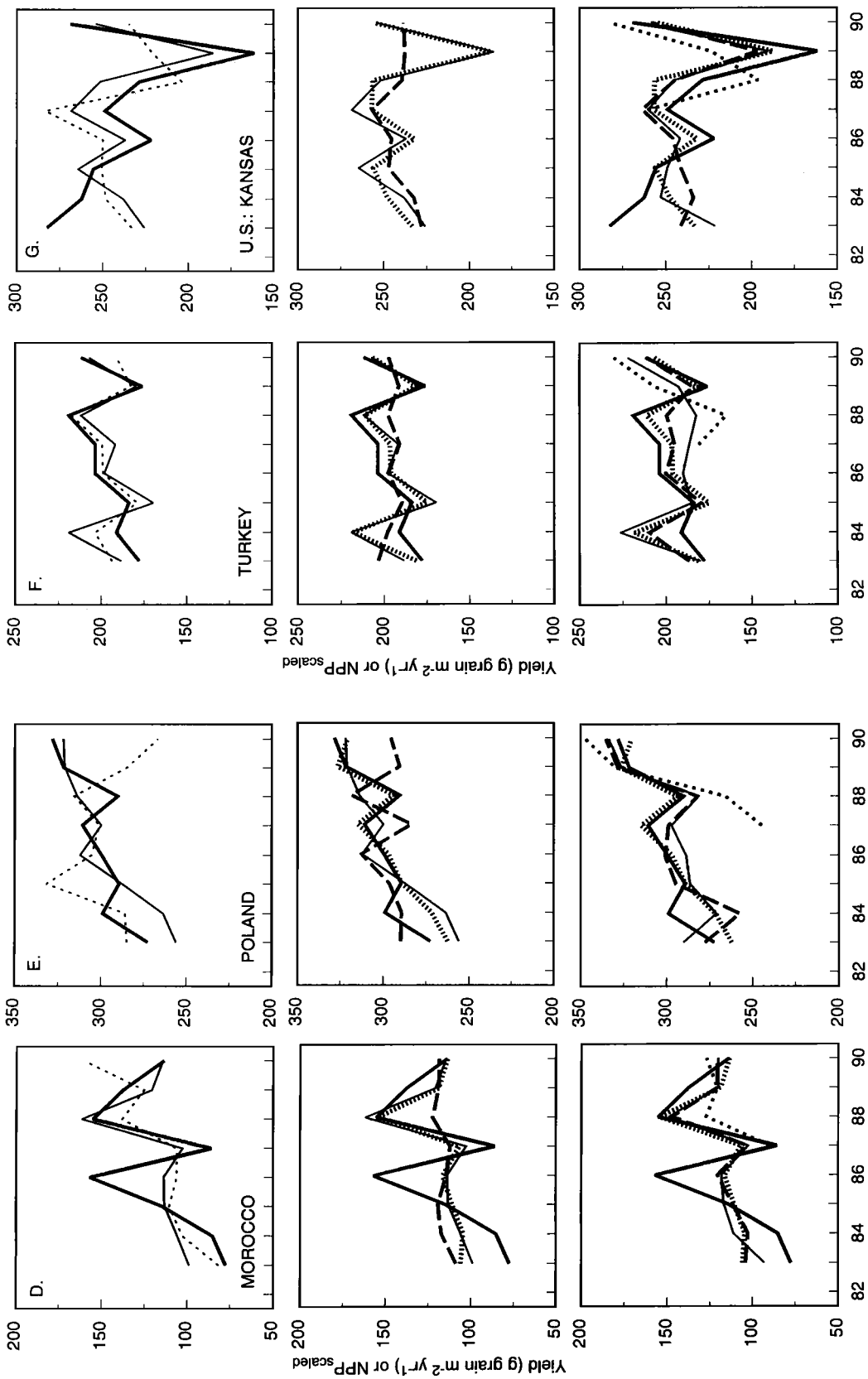

Figure 3. (continued)

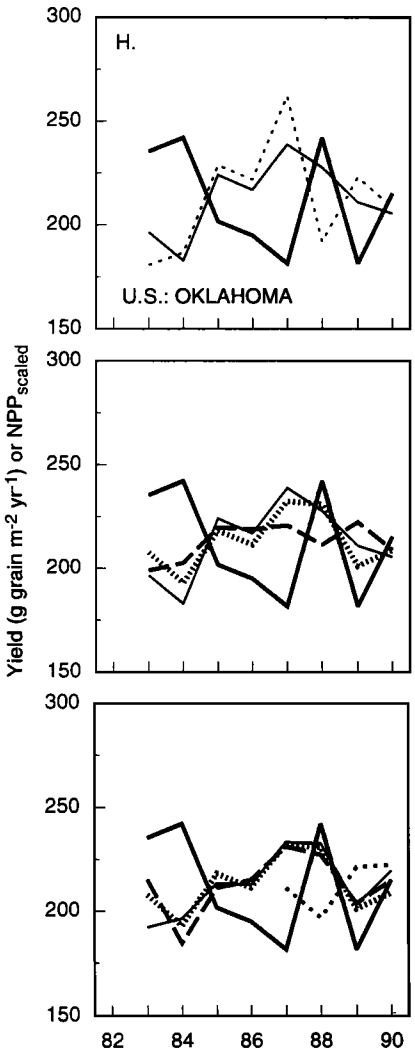

Figure 3. (continued)

candidate sites in India, for example, because of the recent trend toward rice-wheat doublecropping in that region [*Woodhead et al.*, 1994].

Real variation in the NPP-to-yield relationship may arise several ways. Severe cold, disease [*Comeau and Barnett*, 1979], or drought [*Davidson and Birch*, 1978] can substantially lower harvest index, particularly if occurring after anthesis [*Passioura*, 1977] Alternatively, in times of severe crop loss, farmers may harvest only the better fields and thus keep yield numbers (when calculated as production per harvested area) artificially high. That NPP estimates are not as low as yields in poor crop years in South Australia and Saskatchewan (Figure 3) may reflect the effects of drought on harvest index, since both regions are vulnerable to end-of-season drought that affects seed set and grain filling more strongly than biomass production. The large discrepancy between the high NPP estimates and the low grain yields in Oklahoma in 1987 may also reflect the effects of extreme meteorological events on harvest index. That year, at the end of a season of plentiful moisture, Oklahoma experienced an extraordinarily dry April, which limited head filling, followed by grain-destroying floods in May and June [*Oklahoma Department of Agriculture, Oklahoma Agricultural Statistics Service*, 1987a, b].

At the forested site, mismatches between NPP estimates and the tree ring data could be caused by similar factors: errors in the data sets, weaknesses in the models, natural variation in allocation patterns, and contamination of the NDVI signal by secondary species. In addition, error may be caused by having to extrapolate from the stand-level scale of the tree ring data to the grid-cell scale of the model estimates; this source of error is minimized at the agricultural sites because the production data were available at the grid cell scale.

At the boreal forest site the most interesting question regarding error is why there is a trend in the NDVI-based estimates not seen in the tree ring data (Figure 4 and Appendix B). Over the long-term (1805 to present), there is an increase in spruce ring width at the Fort Richardson site, associated with warming temperatures (G.P. Juday and S.A. Marler, manuscript in preparation, 1997), but it is not evident for the 1980s. Possible causes of the difference between trends in NDVI-based NPP estimates and in ring widths include (1) error in extrapolating from the sample to the grid cell: The data used represent stand-level measurements of the dominant species, but the stands sampled may not be fully representative of the grid-cell-level population because the data were originally gathered for a purpose other than grid-cell-level comparisons; and (2) artifactual trend in the NDVI series. Additional sampling of forest growth patterns would help identify which cause is more likely.

3.1.2.4. Differences between NDVI versions: Because CASA's estimates strongly depend on NDVI, we compared the results of using four different NDVI versions in runs where climate was held constant: FASIR (discussed above in section 3.1.2.2), PRE, Pathfinder, and CESBIO (1986-1990 only). There are similarities among the versions. As FASIR does, PRE and Pathfinder describe yield patterns better than the Miami model (Figures 3a-3h, bottom panels, and Table 3). In the same manner as FASIR, PRE and Pathfinder also show positive trends at the boreal site but are correlated with radial growth when detrended (Figures 4a and 4b and Table 4). None of the versions predict Oklahoma wheat yield.

However, the versions also differ. The FASIR estimates are strongly correlated with yield in five of the seven agricultural sites (South Australia, Morocco, Poland, Turkey, and Kansas) and somewhat correlated ($0.05 < P \leq 0.10$) in Saskatchewan (Table 3). PRE is strongly correlated with yield at a slightly different set of five agricultural sites (South Australia, Canada, Morocco, Poland, and Kansas) and somewhat correlated in Turkey. Pathfinder is strongly correlated with yield only at three sites (South Australia, Morocco, and Poland) and somewhat correlated in Canada and Kansas. The CESBIO version is too short to make a quantitative comparison.

Patterns of fit and correlation coefficients can also be compared site by site. This comparison indicates that FASIR describes interannual variation in yields more closely than PRE in four of the seven agricultural sites: South Australia, Kansas, Poland, and Turkey (Figure 3 and Table 3). In Morocco and Saskatchewan, PRE describes yield variation more closely than FASIR. Pathfinder never describes the closest fit to the yield data at any of the agricultural sites and does particularly poorly with Turkish wheat. The short

Table 3. Pearson Correlation Coefficients and P Values for Comparisons of Yield Data and NPP Estimates for 1982-1990 Produced by the CASA Model and the Miami Model

	Standard CASA: Variable FASIR and Variable Climate (Run 1)	CASA: Variable FASIR NDVI (Run 2)	CASA: Variable PRE NDVI (Run 3)	CASA: Variable Pathfinder NDVI (Run 4)	CASA: Variable Climate (Run 5)	Miami (Run 6)
South Australia wheat	0.915 P=0.001	0.862 P=0.003	0.776 P=0.014	0.802 P=0.009	0.804 P=0.009	0.801 P=0.009
Canada: Saskatchewan wheat	0.853 P=0.003	0.586 P=0.097	0.743 P=0.002	0.609 P=0.082	0.827 P=0.006	0.542 P=0.131
Morocco wheat and barley	0.733 P=0.039	0.728 P=0.040	0.839 P=0.009	0.805 P=0.016	0.619 P=0.102	0.484 P=0.225
Poland total grain	0.716 P=0.046	0.887 P=0.003	0.769 P=0.026	0.773 P=0.024	-0.215 P=0.609	-0.488 P=0.220
Turkey wheat	0.641 P=0.087	0.703 P=0.052	0.675 P=0.066	0.160 P=0.705	0.122 P=0.773	0.690 P=0.058
U.S.: Kansas wheat	0.651 P=0.080	0.762 P=0.028	0.729 P=0.040	0.676 P=0.066	-0.154 P=0.715	0.318 P=0.443
U.S.: Oklahoma wheat	-0.548 P=0.160	-0.185 P=0.661	-0.258 P=0.537	-0.250 P=0.550	-0.871 P=0.005	-0.893 P=0.003

In run 1 (standard), the CASA model was driven with time series of air T, PPT, surface solar irradiance, and FASIR NDVI. In runs 2-4 the CASA model was driven with a time series of the NDVI version indicated, and with mean values (1982-1990) of air T, PPT, and surface solar irradiance. In run 5 CASA was driven with time series of the three climatological variables, and with mean FASIR NDVI (1982-1990). In run 6 the Miami model was driven by the time series of air T and PPT.

CESBIO series is the most different of the four. It generally predicts a sharp transition from low to high yields between 1988 and 1989, the time of the NOAA 9 to NOAA 11 transition. For Canada and South Australia, two sites where yields in fact follow this pattern, the CESBIO estimates match well. However, for the remaining five agricultural sites, the CESBIO estimates are poor.

The FASIR processing appears to eliminate artifactual features present in the other NDVI data sets. In Turkey and Poland, for example, the estimates based on the CESBIO, Pathfinder, and PRE NDVI decline from 1986-1988, paralleling NOAA 9's drift to later equatorial crossing times but deviating from the yield data. This decline is absent in the FASIR product, which matches the yield data (Figures 3g and 3f).

Across the sites there is a pattern of systematic mismatches between the NDVI-based estimates and yield data in 1983-1984, during the tenure of NOAA 7 (Figure 3). In Saskatchewan, for example, 1984 yields are overestimated by PRE, more so by FASIR and Pathfinder. The overestimation does not appear to be due to contaminating signals from crops other than wheat, as both barley and canola yields follow the wheat yields for this period (Figure 5). Likewise, 1984 yields in Turkey are overestimated by PRE and to a greater degree by FASIR and Pathfinder. This overestimation is not due to the barley signal (Figure 5). In contrast, 1984 yields are underestimated by all three versions in Kansas, Oklahoma, and Poland (Figure 3).

3.1.3. Summary. The CASA model produces reasonable estimates of mean production and interannual variation at the agricultural test sites. CASA's estimates more closely reproduce yield variation than do estimates by the Miami model, which predicted yield variation at only two sites. Production estimates produced by a light use efficiency model like CASA strongly depend on the quality of the NDVI data used to drive it. Estimates based on the FASIR NDVI generally better reproduced yield patterns than did estimates based on the CESBIO, PRE, or Pathfinder NDVI. Features correlated with change in satellite overpass time in the CESBIO, PRE, and Pathfinder production estimates during the tenure of NOAA 9 were absent from the FASIR estimates. However, a pattern of systematic mismatches between estimates and yield data suggests that all of the longer NDVI versions have difficulties with 1983-1984, during the tenure of NOAA 7. At the boreal site, CASA's estimates were correlated with interannual variation in radial tree growth only when a positive trend was removed from the NDVI data.

3.2. Biome and Global-Scale Comparisons

3.2.1. Negative correlation with equatorial crossing time. Differences between the NDVI versions become more striking at larger scales. At the global scale, the NPP estimates based on the PRE, Pathfinder, and CESBIO NDVI show strong negative correlation with equatorial crossing time (ECT), which reflects both the orbital drift of each satellite and switches between satellites (Figure 6 and Table 6). The FASIR-based estimates show less correlation. PRE estimates decline from 1982 to 1984, following the drift of NOAA 7 from a mean equatorial crossing time of 14.75 hours to 15.69 hours. With the switch to NOAA 9 in 1985 the estimates rise, then fall through 1988 as equatorial crossing time drifts from 14.74 to 15.61 hours, and jump again in 1989 with the switch to NOAA 11 and an earlier equatorial crossing time of 13.80 hours. In the Pathfinder series the 1984 dip is less evident (probably because this version was not corrected for the effects of El Chichón in 1982-1983), but from 1985 on the estimates follow the PRE series and the change in

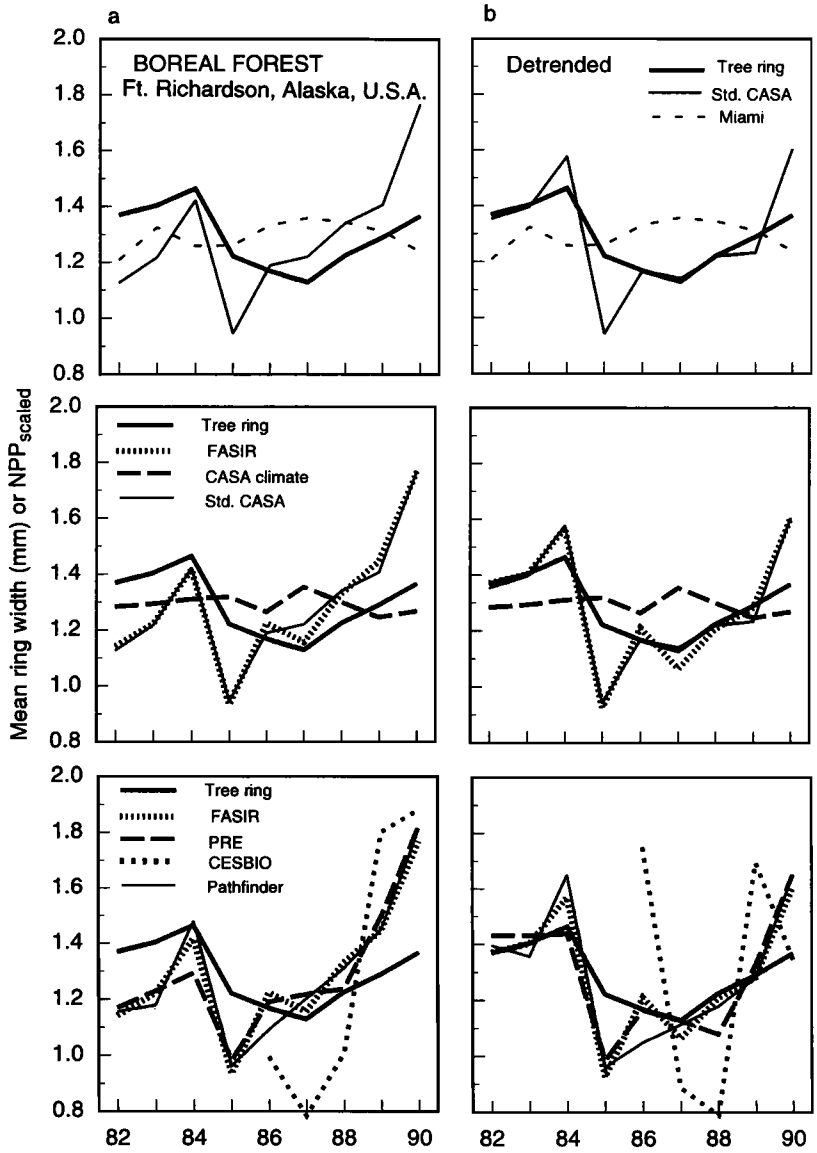

Figure 4. Comparisons of tree ring data and NPP estimates. (a) With trends in NDVI-based estimates and (b) with NDVI-based estimates detrended. The scales of the graphs are identical. To make visual comparisons easier, NPP estimates are scaled to the tree ring data. For each site, NPP_{scaled} = NPP (mean ring width/mean NPP), where the means are the means (1982-1990) at that site. (top panels) Weighted average of tree ring data and NPP estimates produced by standard CASA run and the Miami model, scaled by mean to the tree ring data. (middle panels) Contribution of components of standard CASA run. Tree ring data and scaled estimates produced by the standard CASA run, variable FASIR NDVI, and the CASA climate algorithm. (bottom panels) Comparison of NDVI versions. Tree ring data and scaled estimates produced by variable NDVI CASA runs with the FASIR, PRE, Pathfinder, and CESBIO versions.

equatorial overpass time, as do the CESBIO estimates. The FASIR version does not show features correlated with the drift of NOAA 9, but retains the 1984 dip.

Analysis by vegetation class indicates that equatorial crossing time is strongly negatively correlated with the PRE and Pathfinder estimates of total NPP for low latitude and midlatitude forest ecosystems (Figure 7 and Table 7): tropical rainforest (class 1), broadleaf deciduous trees (class 2), broadleaf and needleleaf trees (class 3), and broadleaf trees with ground cover (class 6), and somewhat with cultivation (class 12). The FASIR estimates are significantly negatively correlated with equatorial crossing time only for classes 1 and 6, and the correlations are weaker than for either PRE or Pathfinder. Equatorial crossing time is not significantly correlated with any NDVI-based estimates of total NPP for the boreal forests (classes 4 and 5) or the short-statured classes: grasslands (class 7), broadleaf shrubs with bare soil (class 9), tundra (class 10), and deserts (class 11). A few weaker correlations are evident, however: ECT is somewhat negatively correlated with PRE estimates of NPP for the boreal forests (classes 4 and 5) and with Pathfinder estimates for the grasslands (class 7) and deserts (class 11). Within these

Table 4. Comparisons of Tree Ring Data and NPP Estimates for 1982-1990 Produced by the CASA Model and the Miami Model: Trends and Pearson Correlation Coefficients

	Standard CASA: Variable FASIR and Variable Climate (Run 1)	CASA: Variable FASIR NDVI (Run 2)	CASA: Variable PRE NDVI (Run 3)	CASA: Variable Pathfinder NDVI (Run 4)	CASA: Variable Climate (Run 5)	Miami (Run 6)
Trends	+10.2 or +4.8% P=0.063	+10.5 or +4.7% P=0.072	+9.7 or +5.0% P=0.046	+10.7 or +4.8% P=0.089	no trend	no trend
Weighted (1:1.2) spruce-birch average based on raw ring widths	0.390 P=0.299	0.419 P=0.262	0.336 P=0.376	0.469 P=0.202	-0.280 P=0.466	-0.621 P=0.074
	0.813[a] P=0.008	0.828[a] P=0.006	0.791[a] P=0.011	0.858[a] P=0.003	n.a.[a]	n.a.[a]
Weighted (1:1.2) spruce-birch average based on detrended ring widths (see Appendix B)	0.808[a] P=0.008	0.821[a] P=0.007	0.829[a] P=0.006	0.873[a] P=0.002	-0.314 P=0.411	-0.647 P=0.059

In run 1 (standard) the CASA model was driven with time series of air T, PPT, surface solar irradiance, and FASIR NDVI. In runs 2-4 the CASA model was driven with a time series of the NDVI version indicated, and with mean values (1982-1990) of air T, PPT, and surface solar irradiance. In run 5 CASA was driven with time series of the three climatological variables, and with mean FASIR NDVI (1982-1990). In run 6 the Miami model was driven by the time series of air T and PPT. Trends (mean annual increase) in NPP estimates are estimated as slope of best fit regression line and given in g C $m^{-2} yr^{-1}$ and as percentage of 1982 NPP.

[a]Value for comparison with detrended NPP estimates

vegetation classes, some regions show stronger correlations than the class as a whole. Most notably, 47% of the boreal forest region shows negative correlation (R≤-0.5) of ECT with PRE-based NPP estimates and 23% with Pathfinder-based estimates (data not shown).

Negative correlation between equatorial crossing time and NDVI-based NPP estimates does not appear to result from coincidental correlation between changes in equatorial crossing time and in climate factors controlling production. Mean annual equatorial crossing time is not correlated with total annual precipitation or mean annual temperature at the global level or for any vegetation class except shrub desert (class 9: R=0.668, P=0.049).

Instead, negative correlation between equatorial crossing time and NDVI-based estimates suggests there may be artifactual signal in some of the NDVI series. Change in equatorial crossing time alters NDVI by changing solar zenith angle (SZA) [*Deering and Eck,* 1987]. Of the four NDVI versions examined, only the FASIR version explicitly corrects for changes in solar zenith angle; the Pathfinder, PRE, and CESBIO versions simply remove values at extreme solar zenith angle. At the agricultural sites where NPP estimates based on the PRE, Pathfinder, and CESBIO NDVI deviated from yields in parallel with the inverse of equatorial crossing time, the FASIR-based estimates did not deviate but instead followed the yield patterns. Similarly, for the agricultural vegetation class as a whole (Table 7), equatorial crossing time is well correlated (negatively) with PRE-based NPP estimates (R=-0.733, P=0.025), somewhat correlated with Pathfinder-based estimates (R=-0.625, P=0.072), and uncorrelated with estimates based on FASIR (R=-0.196, P=0.613).

Table 5. Semipartial Correlation Coefficients for Linear Regression of CASA Estimates Based on Variable FASIR NDVI or on Variable Climate Against Estimates Based on the Standard CASA Run (Both FASIR and Climate Variable)

	CASA: Variable FASIR NDVI	CASA: Variable Climate
South Australia wheat	0.825	0.252
Canada: Saskatchewan wheat	0.620	0.592
Morocco wheat and barley	0.854	0.204
Poland total grain	0.907	0.465
Turkey wheat	0.887	0.246
U.S.: Kansas wheat	0.872	0.281
U.S.: Oklahoma wheat	0.728	0.454

Correlation with equatorial crossing time also leads to estimates of between-year changes in NPP that are markedly greater than estimates based on deconvolutions of atmospheric fluxes. Pathfinder, PRE, and CESBIO predict between-year changes in NPP as large as 7.2-14.0 Gt C (Table 6), 180-360% greater than the largest change in NPP in a flux-based estimate (3.9 Gt C in the *Keeling et al.*[1995]-based estimates [*Thompson et al.*, 1996]; Figure 6). In contrast, the largest between-year change predicted by FASIR is 4.2 Gt C, comparable to that in the flux-based estimates.

Change in equatorial crossing time might be a surrogate for another factor with a similar temporal profile. One candidate would be sensor calibration (reflecting both initial calibration differences and subsequent sensor degradation), but changes in sensor calibration during the life of NOAA 9 and 11 lead to increases, not decreases, in NDVI [*Los et al.*, 1994], and this error source has been addressed to some degree in all four NDVI versions. Furthermore, the FASIR and PRE versions share the same corrections for sensor calibration and degradation (as

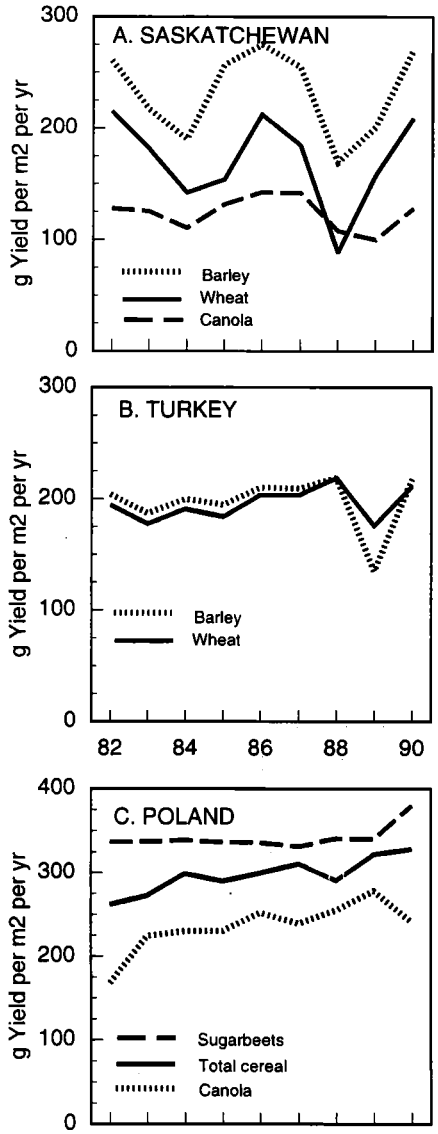

Figure 5. Yields of main and secondary crops. (a) Saskatchewan: yields of the secondary crops barley (R=0.860, P=0.003) and canola (R=0.671, P=0.048) are well correlated with wheat yield. (b) Turkey: yields of barley, the second most extensively planted crop, are well correlated with those of the primary crop, wheat (R=0.799, P=0.010). (c) Poland: note sugarbeets are 1/10th scale. Even though the yield patterns of the cereal grains and the two secondary crops are dissimilar, it is clear that the 1984 dip seen in Poland in the NDVI series cannot be attributed to canola or sugarbeet signals.

well as for the El Chichón aerosols) but differ demonstrably in correlation with equatorial crossing time.

It is not surprising that correlation between equatorial crossing time and NPP estimates is a function of vegetation type (Table 7 and Figure 7). The effect of changes in solar zenith angle on NDVI varies strongly with canopy structure, view angle, atmospheric scattering and absorption, and latitude [*Deering and Eck*, 1987; *Singh*, 1988a, b; *Gutman*, 1991; *Privette et al*, 1995]. We note that correlation with ECT is generally greatest for tall-statured systems, where NDVI is relatively large. This pattern may result from differences in canopy anisotropy or because changes in solar zenith angle may have the greatest effect on NDVI when NDVI is large [*Singh*, 1988a]. Correlation is less strong for tall-statured systems at high latitudes. In high latitude systems, NDVI-based NPP estimates are likely to be affected somewhat

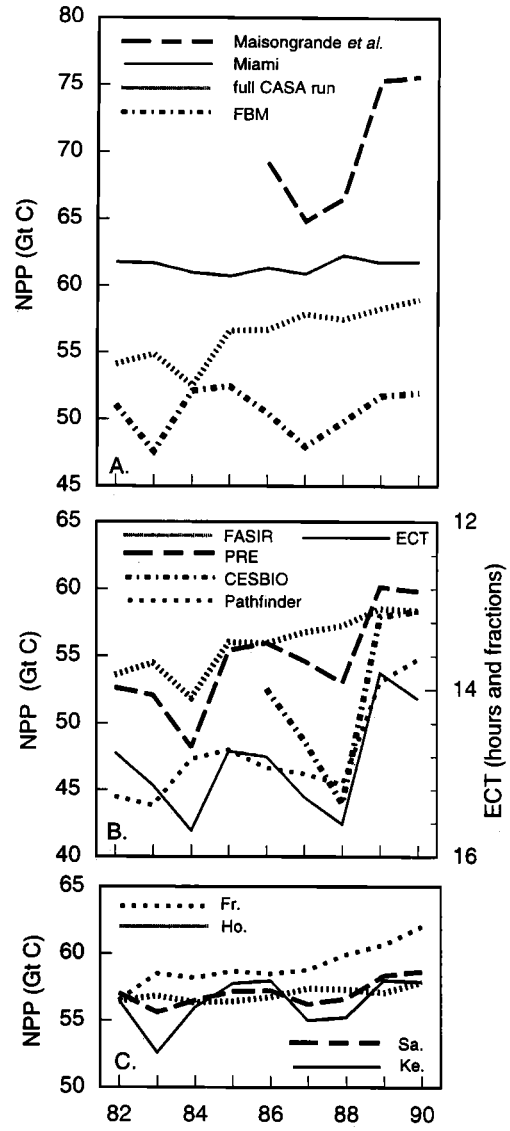

Figure 6. Annual global NPP (Gt C). The scales of the three graphs are identical but offset vertically. (a) Estimates produced by the standard CASA model run with FASIR, by the Miami model, by the Frankfurt Biosphere Model [*Kindermann et al.*, 1996], and by *Maisongrande et al.* [1995] (see Appendix D for notes on the last two). (b) Comparison of NDVI versions. Estimates produced by variable NDVI runs of CASA, using the FASIR, PRE, Pathfinder, and CESBIO NDVI versions. Also graphed is annual mean equatorial crossing time in hours and fractions (solid line, inverted scale). (c) Estimates of variation in NPP [*Thompson et al*, 1996] necessary to match the sinks estimated by *Houghton* [1993] (Ho.), *Francey et al.* [1995] (Fr.), *Keeling et al.* [1995] (Ke.), and *Sarmiento et al.* [1995] (Sa.).

Table 6. Comparison of Estimates of Total Global Net Primary Production

Model Run	Variable Input	Mean, Gt C	CV	Largest Between-Year Change	Trend, Gt C yr^{-1}	Correlation with Equatorial Crossing Time
Standard CASA	climate and NDVI	56.4	3.8%	84-85: 4.12 Gt C	0.69 or 1.2% P=0.002	-0.551 P=0.124
FBM	climate	50.6	3.5%	83-84: 4.5 Gt C	0.12 or 0.2% P=0.647	-0.424 P=0.255
Miami	climate	61.5	0.9%	87-88: 1.41 Gt C	0.05 or 0.08% P=0.474	-0.178 P=0.646
CASA: variable FASIR	NDVI	55.9	4.0%	84-85: 4.16 Gt C	0.72 or 1.3% P=0.002	-0.604 P=0.085
CASA: variable PRE	NDVI	54.7	6.9%	84-85: 7.19 Gt C	1.03 or 1.9% P=0.021	-0.885 P=0.002
CASA: variable Pathfinder	NDVI	47.7	7.9%	88-89: 7.69 Gt C	1.06 or 2.2% P=0.016	-0.756 P=0.018
CASA: variable CESBIO	NDVI	52.3	11.8%	88-89: 13.97 Gt C	2.09 or 4.0% P=0.350	-0.975 P=0.005
Maisongrande: CESBIO	NDVI	70.3	7.1%	88-89: 8.8 Gt C	2.33 or 3.3% P=0.152	-0.948 P=0.014

Trends (mean annual increase) in NPP estimates are estimated as slope of best fit regression line and given in Gt C yr^{-1} and as percentage of 1982 NPP.

differently by changes in solar zenith angle than those at lower latitudes because the interannual variation in solar zenith angle caused by changes in satellite overpass time is somewhat less at high latitudes than at low latitudes [*Privette et al.*, 1995]. Additionally, during winter and shoulder-season months at high latitudes, late overpass times can lead to solar zenith angles so extreme that atmospheric effects will dominate the NDVI signal [*Holben*, 1986] or NDVI data will be missing altogether.

3.2.2. Trends. The suggestion of artifacts in the NDVI series opens the question of the source of the positive global-scale trends seen in the NDVI-based estimates (Table 6) [*Malmström et al.*, 1995; *Myneni et al.*, 1997]. There are no significant trends in global-scale estimates produced by the Miami model or the Frankfurt Biosphere Model [*Kindermann et al.*, 1996] (see Appendix D), which are based on meteorological data. With the NDVI-based estimates, the global trends range from +0.69 Gt C yr^{-1} (or +1.2% per year) with the standard CASA run (variable climate, variable FASIR NDVI) to +1.06 Gt C yr^{-1} (or +2.2% per year) with variable Pathfinder NDVI, and are significant in all cases (Table 6 and Figure 6). Pathfinder and PRE produce larger trends than does FASIR. Because the CESBIO NDVI used here covers only 5 years, its trends are more difficult to evaluate. The slope of the best fit line is about twice as steep as that for the other NDVI runs, but with the small n it is not significantly different from zero. Estimates produced by the *Maisongrande et al.* [1995] model (see Appendix D), also based on CESBIO NDVI, show similar patterns of variation.

Positive trends are evident for all the vegetation classes except the desert classes 9 and 11 (Table 8 and Figure 7) but vary in magnitude with the NDVI version. On a percent per year basis, the trends are generally largest for the high latitude systems.

Because satellite radiometers give information about the integrated response of plant canopies to environmental factors, NDVI-based models of NPP can capture the responses of vegetation to factors not included in models relying exclusively on meteorological data. Among these could be responses to N deposition or to increases in atmospheric carbon dioxide. Do the trends observed here reflect biological change, unidentified artifact, or both? The trends are evident even in FASIR, the NDVI version that appears to have the greatest amount of artifact removed.

Certainly, factors like CO_2 or N fertilization have the potential to induce trends in NPP. *Luo and Mooney* [1996], for example, use an instantaneous derivative of the *Farquhar et al.* [1980] photosynthesis model to estimate that a 1-ppm change in CO_2 levels at 357 ppm would increase photosynthetic carbon uptake 0.115% to 0.248%. Carbon dioxide concentrations rose on average 1.62 ppm per year between 1982 and 1990 [*Keeling and Whorf*, 1991]. If it is assumed that gross primary production (GPP) equals twice NPP (and that this relationship is unchanged by small increases in CO_2 concentrations) and if the FASIR-based CASA estimates of NPP are used, Luo and Mooney's algorithm would predict an increase in global NPP between 0.10 and 0.23 Gt C yr^{-1}, one-seventh to one-third of the rate estimated by CASA driven with FASIR (Table 6). This high-end estimate of CO_2 response does not consider temperature interactions or ecological or physiological feedbacks affecting the relationship between photosynthetic response and production.

At our agricultural test sites there was no evidence of artifactual trends in the comparison of yield and NDVI-based NPP estimates (Figure 3). At six of the seven sites there was no trend in either yield or estimates. In Poland the positive trend in total cereal yield was matched by trend in the FASIR-based estimates (but was not captured by the Miami model). Thus the trend seen in the FASIR-based estimates for agriculture as a whole, 1.4% per year, may reflect actual production increases. However, the contribution of biological change or artifact may vary by biome, and agriculture does not represent all biomes. At our one nonagricultural site, in the boreal forest, the NDVI-based estimates showed a positive

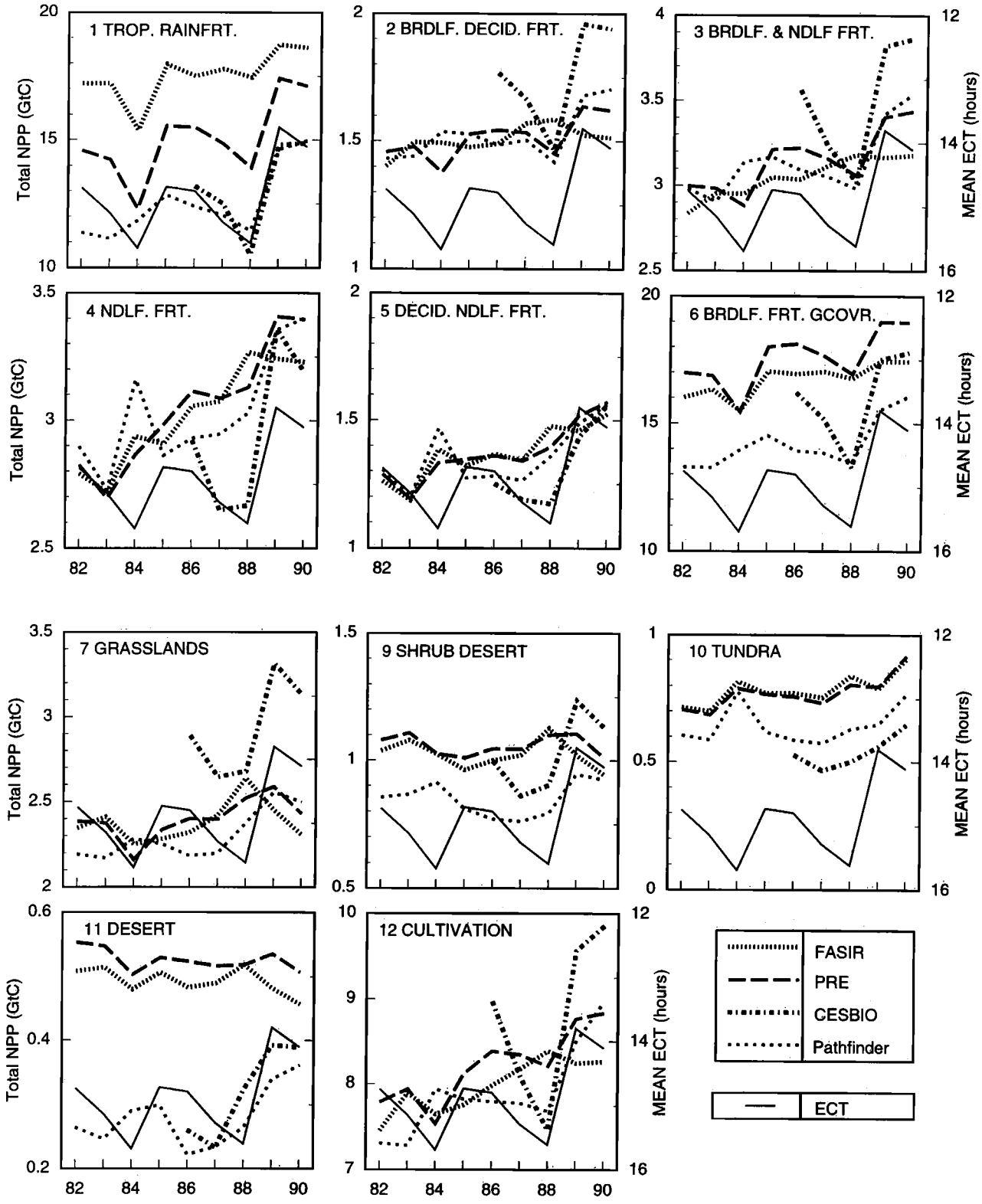

Figure 7. Comparison of estimates of total NPP for each vegetation class from variable NDVI runs of CASA using the FASIR, PRE, Pathfinder, and CESBIO versions. Also shown is the NOAA equatorial crossing time (inverted scale).

Table 7. Pearson Correlation Coefficients for Equatorial Crossing Time of NOAA Satellites (7, 9, and 11) and CASA NPP Estimates for 1982-1990 Produced by Different NDVI Versions, by Vegetation Class

	CASA: Variable FASIR NDVI	CASA: Variable PRE NDVI	CASA: Variable Pathfinder NDVI
Tall-statured systems			
1. Tropical rainforest	-0.790 P=0.011	-0.937 P<0.000	-0.838 P=0.005
2. Broadleaf deciduous forest	0.234 P=0.544	-0.877 P=0.022	-0.740 P=0.023
3. Broadleaf and needleleaf forest	-0.287 P=0.454	-0.848 P=0.004	-0.753 P=0.019
4. Needleleaf forest	-0.297 P=0.438	-0.640 P=0.063	-0.518 P=0.153
5. Deciduous needleleaf forest	-0.299 P=0.434	-0.639 P=0.064	-0.421 P=0.259
6. Broadleaf with ground-cover	-0.673 P=0.047	-0.868 P=0.002	-0.779 P=0.013
Short-statured systems			
7. Grasslands	0.180 P=0.644	-0.546 P=0.129	-0.596 P=0.090
9. Shrub desert	0.579 P=0.103	0.019 P=0.961	-0.488 P=0.183
10. Tundra	-0.171 P=0.660	-0.375 P=0.321	-0.088 P=0.823
11. Deserts	0.482 P=0.188	-0.250 P=0.516	-0.643 P=0.062
Variable stature			
12. Cultivation	-0.196 P=0.613	-0.733 P=0.025	-0.625 P=0.072

trend (4.7-5.0%) not evident in the tree ring data (Figure 4 and Table 4). The discrepancy may reflect either error in extrapolating the tree ring data to the grid-cell scale or artifact in the NDVI data, or both.

Estimates of increases in NPP can also be constrained by analysis of atmospheric CO_2 fluxes. Trend in NPP may be necessary to explain terrestrial sinks, especially if over a period of decades. The mean increase in total global NPP from 1880-1990 necessary to sustain the sink estimated by *Houghton*'s [1993] or *Sarmiento et al.*'s [1995] deconvolutions of atmospheric fluxes is ~0.1 Gt C yr^{-1} [*Thompson et al.*, 1996]. The mean rate of increase for 1982-1990 would be slightly higher, 0.16 Gt C yr^{-1} (0.3% yr^{-1}) for the Houghton-based estimate and 0.238 Gt C yr^{-1} (0.4% yr^{-1}) for the Sarmiento et al.-based estimate (Figure 6). These values are one-fourth to one-third of the rate estimated by CASA driven by FASIR (Table 6). The trend in NPP estimates based on FASIR, PRE, or Pathfinder is significantly greater than the trend estimated from either the Houghton or Sarmiento et al. deconvolutions (Table 9).

Increases in NPP are also likely to contribute to observed increases in the amplitude of the seasonal cycle of atmospheric CO_2. The most conservative NDVI-based estimate of trends in global NPP (standard CASA: +1.2% yr^{-1}, Table 6) is approximately 2 times greater than the rate necessary to explain the 0.66% yr^{-1} mean amplitude increase observed during the 1980s at the five NOAA/CMDL stations north of 55°N (J.T. Randerson et al., The contribution of terrestrial sources and sinks to trends in the seasonal cycle of atmospheric carbon dioxide, submitted to *Global Biogeochemical Cycles*, 1997). However, even a 0.6% yr^{-1} global increase in NPP would lead to a net terrestrial uptake of ~5.0 Gt C yr^{-1}, roughly 2.5 times the estimated mean value for the 1980s [*Schimel et al.*, 1995]. To be consistent with both the northern amplitude increases and estimates of net terrestrial uptake, NPP trends would need to be limited to ~0.6% yr^{-1} and localized north of 30°N. With the NDVI-based estimates, however, trends are greater than this and evident in most biomes, including those south of 30°N (Table 8).

Thus the existence of trends in CASA's NDVI-based NPP estimates is consistent with potential stimulation of terrestrial production by factors such as CO_2 enrichment, N fertilization, or temperature warming, but the magnitude of the global trends seen in these estimates is significantly greater than suggested by constraints imposed by atmospheric fluxes.

To determine how much of the trend in each biome reflects biological change, the NDVI series should be reexamined to evaluate the contribution of potential trend-inducing artifacts. Correlation with equatorial crossing time suggests that solar zenith angle effects persist in the PRE, Pathfinder, and CESBIO NDVI versions. In the FASIR version, these effects are reduced by the application of a solar zenith angle correction, but a trend remains. It is possible that residual solar zenith angle effects persist in the FASIR data. The solar zenith angle correction applied to FASIR 2.1 was derived from a statistical analysis of large populations of NDVI data and is based on the assumption that the effect of solar zenith angle varies linearly with NDVI, having no effect on bare soils and maximum effect when NDVI is high (Appendix C) [*Sellers et al.*, 1996; S.O. Los, manuscript in preparation, 1997]. Ground measurements have shown, however, that a linear relationship may not be appropriate for some land cover types [*Deering et al.*, 1992a, b]. An additional difficulty in developing a solar zenith angle correction is that the effects of other factors may be confounded with the effects of high solar zenith angles. For example, in some regions, cloud buildup is greatest late in the afternoon, the same period when solar zenith angles are largest. Thus NDVI values from late afternoon overpass times may be reduced both by solar zenith angle effects and by cloud cover.

It has been suggested that the effects of solar zenith angle can magnify the effects of sensor degradation [*Goward et al.*, 1991]. Corrections for sensor degradation are generally tested against a time series of desert sites assumed to be time invariant. If there are solar zenith angle effects at these sites, these can present a problem when deriving the sensor degradation correction. Solar zenith angle effects in the NDVI over bare soils were not seen in the 9-year PRE or FASIR time series [*Los*, 1997, also manuscript in preparation, 1997]. An earlier analysis [*Sellers et al.*, 1996] did find a small solar zenith angle effect over bare soils, but this analysis was based only on data for 1987.

A third possibility is that the correction for the El Chichón aerosols in the PRE and FASIR versions (Appendix C) is incomplete. (The Pathfinder version was not corrected for

Table 8. Mean Annual Increase in NPP Estimates for 1982-1990 in Gt C yr^{-1} and as Percentage of 1982 NPP

	Standard CASA: Variable FASIR and Variable Climate	CASA: Variable FASIR	CASA: Variable PRE	CASA: Variable Pathfinder	Miami
Tall-statured systems					
1. Tropical rainforest	0.234 or 1.3% P=0.054	0.237 or 1.4% P=0.052	0.371 or 2.5% P=0.064	0.388 or 3.4% P=0.017	0.040 or 0.3% P=0.158
2. Broadleaf deciduous forest	0.012 or 0.8% P=0.064	0.014 or 1.0% P=0.04	0.022 or 1.5% P=0.031	0.026 or 1.8% P=0.041	0.000 or 0% P=0.949
3. Broadleaf and needleleaf forest	0.043 or 1.4% P<0.001	0.042 or 1.5% P=0.001	0.055 or 1.8% P=0.010	0.056 or 1.9% P=0.026	0.003 or 0.1% P=0.722
4. Needleleaf forest	0.073 or 2.6% P<0.001	0.069 or 2.5% P=0.001	0.085 or 3.0% P<0.001	0.062 or 2.1% P=0.021	0.027 or 0.8% P=0.095
5. Deciduous needleleaf forest	0.034 or 2.7% P=0.004	0.035 or 2.8% P=0.002	0.037 or 2.9% P=0.001	0.028 or 2.1% P=0.074	0.014 or 1.3% P=0.211
6. Broadleaf with ground-cover	0.171 or 1.1% P=0.018	0.193 or 1.2% P=0.009	0.282 or 1.7% P=0.043	0.270 or 2.0% P=0.022	-0.008 or 0% P=0.753
Short-statured systems					
7. Grasslands	0.015 or 0.6% P=0.384	0.015 or 0.6% P=0.358	0.027 or 1.1% P=0.076	0.042 or 1.9% P=0.010	0.006 or 0.1% P=0.558
9. Shrub desert	-0.009 or -0.8% P=0.284	-0.005 or -0.5% P=0.541	-0.002 or -0.2% P=0.770	0.004 or 0.5% P=0.692	-0.041 or -1.3% P=0.039
10. Tundra	0.014 or 1.9% P=0.052	0.018 or 2.5% P=0.017	0.020 or 2.8% P=0.012	0.008 or 1.3% P=0.429	0.005 or 0.6% P=0.201
11. Deserts	-0.005 or -0.9% P=0.052	-0.004 or -0.8% P=0.124	0.009 or 1.6% P=0.130	0.003 or 1.1% P=0.138	0.003 or 0.2% P=0.880
Variable stature					
12. Cultivation	0.102 or 1.4% P=0.004	0.102 or 1.4% P=0.001	0.137 or 1.8% P=0.002	0.162 or 2.2% P=0.006	0.007 or 0.1% P=0.759

Trends estimated as slope of best fit regression line.

these aerosols, which contribute to the trends evident in estimates based on this version.) This could lower the NDVI values for 1982-1983, thus inducing or enhancing a trend in the time series. However, an El Chichón effect is unlikely to explain the entire trend because (1) the effects of El Chichón aerosols are confined to mid and low latitudes, while trends are more widespread, and (2) the lowest NDVI values in the PRE and FASIR series tend to occur in 1984, by which point the effects of the El Chichón aerosols are minimal [*Vermote et al.*, 1996; S.O. Los, manuscript in preparation, 1997].

Table 9. Comparison of Slopes of Regression Lines for Multiyear Estimates of Global NPP (1982-1990): F_s and P Values

NDVI-Based Estimate	Estimate[a] Based on *Sarmiento et al.* [1995] Deconvolution	Estimate[a] Based on *Houghton* [1993] Deconvolution
Standard CASA	6.53 P < 0.025	12.64 P< 0.005
CASA: variable FASIR	7.35 P < 0.025	13.87 P < 0.005
CASA: variable PRE	4.82 P < 0.05	6.25 P < 0.05
CASA: variable Pathfinder	5.54 P < 0.05	7.19 P=0.025

F_s and P values are calculated according to *Sokal and Rohl* [1981].
[a] From *Thompson et al.* [1996].

4. Conclusions

This investigation demonstrates how agricultural yield data and tree ring data may be used to test estimates of interannual variation in net primary production. We have shown that the CASA model produces reasonable estimates of mean production and interannual variation at agricultural test sites. CASA's estimates more closely reproduce yield variation than do estimates by the Miami model, which has been used to assess variation in production in several previous studies but here predicts yield variation poorly. We have also shown that estimates of interannual variation depend on the NDVI version used. Of the versions we tested, the FASIR NDVI most closely reproduced yield data and showed the least correlation with changes in equatorial crossing time of the NOAA satellites. One issue raised is the source of the positive trends evident in CASA's NDVI-based estimates of global NPP. The existence of trends in these estimates is consistent with potential stimulation of terrestrial production by factors such as CO_2 enrichment, N fertilization, or temperature warming, but the magnitude of the global trends seen is significantly greater than suggested by constraints imposed by atmospheric fluxes. To better constrain estimates of trends, we suggest reexamination of possible sources of artifact in the NDVI series, such as residual solar zenith angle effects.

Appendix A: Sites Selected

For a summary of site characteristics and sources of information, see Tables A1 and A2.

Table A1. Site Characteristics

Region	Center Latitude and Longitude	No. of Grid Cells	Crop Cycle[a] (Agricultural Year Used)	Irrigation
South Australia wheat	138°E, 33°S	16	May-Dec. [*Australian Bureau of Statistics*, 1990] (Jan.-Dec.)	<3% of cropped area [*Australian Bureau of Statistics*, 1990]
Canada: Saskatchewan prairie wheat	106°W, 50°N	31	May-Aug./Sept./Oct. (Jan.-Dec.)	0.2% of total cropland [*Statistics Canada*, 1991]
Morocco wheat and barley	6°W, 33°N	12	Nov./Dec.-May/June (Sept.-Aug.)	~10% of cropped area [*U.S. Department of Agriculture, Foreign Agricultural Service*, 1991]
Poland total cereal grain	20°E, 53°N	28	Sept./Oct.-July/Aug. for wheat; Sept./Oct.-June/July for rye; April-Aug./Sept. for oats (Sept.-Aug.)	<0.7% of arable land [*CIA*, 1995]
Turkey wheat	33°E, 39°N	58	Sept./Oc.t/Nov.-July/Aug. (Sept.-Aug.)	<1% of wheat area (U.S. Department of Agriculture, Foreign Agricultural Service, attaché observation, 1995)
U.S.: Kansas wheat	99°W, 38°N	13	Sept./Oct.-June/July [*Smika*, 1992] (Sept.-Aug.)	~6% of wheat area [*U.S. Department of Agriculture, National Agricultural Statistics Service*, 1995]
U.S.: Oklahoma wheat	98°W, 35°N	11	Sept./Oct.-June/July (Sept.-Aug.)	<5% [*U.S. Department of Agriculture, National Agricultural Statistics Service*, 1993]

[a]Unless noted otherwise, source of information on crop cycle is *U.S. Department of Agriculture, World Agricultural Outlook Board* [1994].

Australia: South Australian wheat region. More than 50% of the crop area in South Australia is planted to wheat [*Australian Bureau of Statistics*, 1994]. The wheat belt includes the Eyre Peninsula and regions to the west along the Great Australian Bight as well as somewhat inland; the Yorke Peninsula and areas inland; and regions near Adelaide. Other crops grown in this area include barley (876,000 ha or 29% of the crop area), oats (4.4% of the area), and grain legumes [*Australian Bureau of Statistics*, 1994]. The wheat belt is a winter rainfall region, where rains are usually reliable during the winter (June-August) but less so during the later part of the wheat growing season (October-November) [*Australian Bureau of Statistics*, 1990; *Van Royen*, 1952]. Because of low soil fertility and the low levels and variability of rainfall, Australian wheat yields tend to be lower than those in Europe and North America and more variable from year to year [*Perry*, 1992]. One of the worst crop years resulted from severe drought during the 1982-1983 ENSO. Average yield increases in recent years have been small and variable [*Lazenby et al.*, 1994].

Canada: Saskatchewan wheat region. The Saskatchewan prairie region produces more than half of the wheat grown in Canada, with Alberta and Manitoba making somewhat smaller contributions [*Statistics Canada*, 1988a]. Wheat is the most extensively planted crop in this province (8,377,000 ha), with barley (1,416,000 ha), canola/rapeseed (1,174,000 ha), and oats (364,000 ha) of secondary importance (1985 figures [*Statistics Canada*, 1988a]). The

Table A2. Sources of Information

Region	Extent of Crop Area	Yield Data
South Australia wheat	*Lazenby et al.* [1994]; *Perry* [1992]	*Australian Bureau of Statistics* [1990, 1994]
Canada: Saskatchewan prairie wheat	*Canadian Wheat Board* [1989, 1994]	*Statistics Canada* [1985, 1987, 1988a, b, 1989, 1990]
Morocco wheat and barley	*U.S. Department of Agriculture, World Agricultural Outlook Board* [1994]	*Food and Agriculture Organization of the U. N.* [1984, 1986, 1989, 1990]
Poland total cereal grain	*U.S. Department of Agriculture, World Agricultural Outlook Board* [1994]	*Food and Agriculture Organization of the U. N.* [1984, 1986, 1989, 1990]
Turkey wheat	*U.S. Department of Agriculture, World Agricultural Outlook Board* [1994]	*Devlet Istatistik Enstitusu* [1987, 1993]
U.S.: Kansas wheat	*Kansas Department of Agriculture, Division of Statistics* [1985]	*U.S. Department of Commerce* [1985, 1987, 1989, 1991, 1992]
U.S.: Oklahoma wheat	*Oklahoma Department of Agriculture, Oklahoma Agricultural Statistics Service* [1987c]	*U.S. Department of Commerce* [1985, 1987, 1989, 1991, 1992]

For Morocco, where barley and wheat contribute about equally to grain production, yield was calculated for each year as the mean of the wheat and barley yields, weighted by area for each crop. Yield figures are based on harvested area except for Turkey, where planted area is used.

region of highest wheat density is farther south in the province than that of these other crops, although some overlap occurs [*Canadian Wheat Board*, 1989, 1994]. Because of the severe winters, most of the wheat is spring wheat (or durham). Severe drought linked to the La Niña in 1988 [*Trenberth et al.*, 1988] brought about one of the worst harvests on record, with the drought effect comparable to that of 1919 and 1937 [*Walker*, 1989]. Yields in 1984, the other La Niña year in this series, were also poor, but both 1982 and 1986 brought record crops. For 1954-1978, Canadian yields were more variable than those in France, India, the United States, and Mexico but slightly less variable than in Australia [*Perry*, 1992].

Moroccan wheat and barley region. Of the estimated 8.6 million arable hectares in Morocco [*U.S. Department of Agriculture, Foreign Agricultural Service*, 1991], about 60% are planted to wheat and barley, approximately equally divided between the two cereals [*U.S. Department of Agriculture, World Agricultural Outlook Board*, 1994]. Little acreage is irrigated, so yields tend to vary with precipitation patterns [*US. Department of Agriculture, Foreign Agricultural Service*, 1991]. Crops of secondary importance are olives, citrus, and pulses [*U.S. Department of Agriculture, Foreign Agricultural Service*, 1991]. Rains here fall in the winter, with the summers becoming hot and dry [*U.S. Department of Agriculture, World Agricultural Outlook Board*, 1994].

Polish cereal grain region. Cereal grains, rye (2,760,000 ha), wheat (2,025,000 ha), barley, oats (924,000 ha), and triticale (1986 figures from *U.S. Department of Agriculture, World Agricultural Outlook Board* [1994]), are planted on more than 50% of Poland's cultivated acreage [*U.S. Department of Agriculture, Foreign Agricultural Service*, 1991]. Secondary crops include potatoes, canola (515,000 ha), and sugarbeet (423,000 ha) (1986 figures from *U.S. Department of Agriculture, World Agricultural Outlook Board* [1994]). The summers here are relatively mild, with precipitation heaviest during the April-October growing season; winters are cold [*U.S. Department of Agriculture, World Agricultural Outlook Board*, 1994]. In 1990, approximately 75% of agricultural production came from small private farms (mean size 6 ha.) [*U.S. Department of Agriculture, Foreign Agricultural Service*, 1991].

Turkish wheat region. Sixty to sixty-five percent of Turkey's land is used for agriculture [*U.S. Department of Agriculture, Foreign Agricultural Service*, 1991]. The most extensively planted crop is wheat (9,435,000 ha in 1988), which covers more than 50% of the total area sown to field crops. Barley is the second most extensively planted crop (3,445,000 ha in 1988), covering an additional ~18% of the total area sown [*Devlet Istatistik Enstitusu*, 1993]. Secondary crops of importance include lentils (983,000 ha), chickpeas (778,000 ha), and cotton (740,000 ha) (1988 figures) [*Devlet Istatistik Enstitusu*, 1993]. Most of the grain is grown dryland, with summer fallow (USDA-FAS, attaché observations, 1995). Precipitation here is typically highest in the winter and spring [*U.S. Department of Agriculture, World Agricultural Outlook Board*, 1994]. Wheat and barley production reached a record high in 1988, but dry weather reduced yields in 1989 [*U.S. Department of Agriculture, Foreign Agricultural Service*, 1991].

U.S.: Kansas wheat region. Located in the Central Great Plains, Kansas produces more wheat than any other state in the United States, harvesting some 4,000,000 ha in 1987 [*U.S. Department of Commerce*, 1991]. Winter wheat is the most extensively planted crop in the state. Notable secondary crops are sorghum (1,568,000 ha harvested for all purposes in 1987 [*U.S. Department of Agriculture, National Agricultural Statistics Service*, 1996]), soybeans (850,000 ha harvested in 1987 [*U.S. Department of Commerce*, 1991]), and corn (498,000 ha harvested in 1987 [*U.S. Department of Commerce*, 1991]). Kansas' climate becomes cooler and more arid as one moves from east to west. Most of the wheat is grown in the drier and cooler western and central districts, where, like most Central Great Plains wheat, it is little irrigated. Irrigation has reached into the western region but is concentrated in the soybean and corn field of the southwest district [*U.S. Department of Agriculture, National Agricultural Statistics Service*, 1995]. The grid cells we selected correspond to the regions of densest wheat planting: the eastern half of the western districts, the central districts, and the northwest section of the eastern districts. The northwestern part of the state has a high density of wheat acreage as well, but this region was not classified as agriculture in the *DeFries and Townshend* [1995] vegetation class map and so, for consistency, was not used here. Wheat yields are quite variable from year to year and dipped precipitously in 1989.

U.S.: Oklahoma wheat region. Located immediately south of Kansas, Oklahoma nonetheless experiences a different climate regime, one that is more subtropical. As a consequence, yield patterns here do not parallel those in Kansas. As in Kansas, winter wheat is the most extensively planted crop, with 2,100,000 ha harvested in 1986 [*Oklahoma Department of Agriculture, Oklahoma Agricultural Statistics Service*, 1987c]. Important secondary crops include sorghum (198,000 ha harvested for grain in 1986 [*Oklahoma Department of Agriculture, Oklahoma Agricultural Statistics Service*, 1987c]), cotton (142,000 ha harvested in 1986 [*Oklahoma Department of Agriculture, Oklahoma Agricultural Statistics Service*, 1987c]), and hay [*U.S. Department of Commerce*, 1984]). We used the Panhandle area and the region east to 97°W, encompassing the west central, southwest, and north central districts and the western halves of the central and south central districts. Wheat yields here were low in 1985-1987 and in 1989.

Appendix B: Tree Ring Data

Data were collected at Fort Richardson, Alaska, U.S.A., within the boreal forest zone. Fort Richardson is a 21,193 ha U.S. Army base that borders the city of Anchorage to the east. Mean annual temperature at the Anchorage airport station is 1.9°C, annual precipitation is 400 mm. Roads, trails, structures, and land clearance have affected less than 7% of the base. Increment cores were collected from 45 plots sampled within undisturbed older forest communities of Fort Richardson. All stands sampled were below 350 m in elevation.

Trees were selected for coring based on occurrence in a randomly placed circular plot. Trees with rotten centers were not successfully cored, but otherwise trees were sampled in

Table B1. Components of Weighted Average of Tree Ring Data: Pearson Correlation Coefficients and P Values for Comparisons with NPP Estimates for 1982-1990 Produced by the CASA Model

	Standard CASA: Variable FASIR NDVI and Variable Climate	CASA: Variable FASIR NDVI	CASA: Variable PRE NDVI	CASA: Variable Pathfinder NDVI	CASA Climate	Miami
Weighted (1:1.2) spruce-birch average	0.813 P=0.008	0.828 P=0.006	0.791 P=0.011	0.858 P=0.003	-0.280 P=0.466	-0.621 P=0.074
Spruce	0.139 P=0.721	0.163 P=0.676	0.191 P=0.623	0.069 P=0.859	-0.022 P=0.956	-0.204 P=0.598
Birch	0.791 P=0.011	0.802 P=0.009	0.756 P=0.018	0.855 P=0.003	-0.279 P=0.467	-0.621 P=0.074

Based on detrended NPP estimates, except for CASA climate and Miami runs, in which trends are not evident.

proportion to their occurrence in older forest. The radial growth history of 197 white spruce (probably hybrid white X Sitka spruce, *Picea x lutzii* Little) and 58 birch trees (*Betula papyrifera*) were measured. Minimum individual tree ages (number of measurable rings) in the spruce sample ranged from 252 to 13 years (mean 100.5, median 96.0). Minimum age of trees in the birch sample ranged from 226 to 19 years (mean 78.0, median 61.5).

Annual ring width to the nearest 0.01 mm was measured at the University of Alaska Fairbanks tree ring laboratory using an optical encoder system. Cores were manually inspected to identify reliable cross-dating series, and about 2% of the cores were not included because of indeterminate dating. Cross-dating was performed by standard dendrochronological techniques [*Fritts*, 1976; *Cook and Kairiukstis*, 1990]. Mean radial growth was calculated using 101 spruce with continuous ring widths from 1900 to 1995 and 17 birch with continuous rings from 1934 to 1995. The reduction in sample size from 58 to 17 birch did not markedly skew the representativeness of the birch diameters; mean air dry diameter of the birch increased from 9.9 to 10.3 cm. Mean spruce diameter (air dry) increased from 11.5 cm in the entire sample of 197 trees to 15.4 cm in the sample of 101.

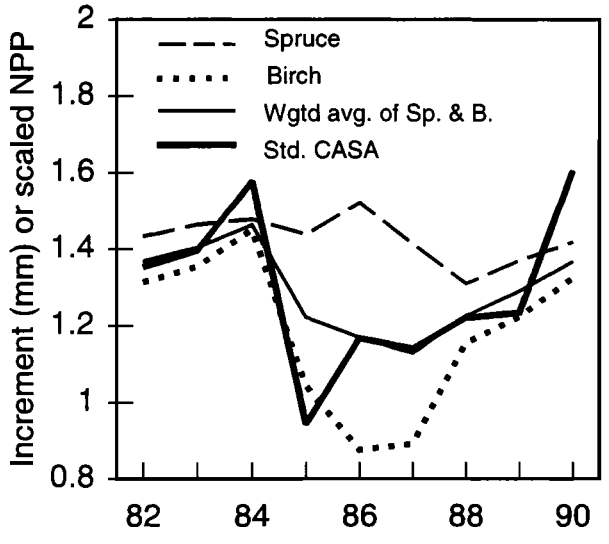

Figure B1. Components of weighted tree ring average and detrended standard CASA run estimates of NPP scaled to the tree ring average. Tree ring average is weighted 1.2 birch to 1.0 spruce, representing the relationship of the area covered by those two species (see Methods).

Standard tree ring chronologies are produced by removing trends related to aging and normalizing widths across trees. Because the goal was to assess stand growth, not to develop climate proxies, raw ring width data were used for calculating the means (Table B1 and Figure B1). All trees selected were beyond the age of juvenile growth distortions, and calculation of a stand average ring-width index would have overweighted the contribution of small trees to total stand growth. To confirm that the lack of trends seen in the mean data was not the result of using raw ring widths, we repeated our analysis using ring widths that had been detrended by standard methods to account for aging. Raw ring width chronologies were processed into detrended series using autoregressive standardization (the ARSTAN method) in which conservative straight line or negative exponential fits were specified for standardization [*Cook*, 1985; *Cook and Kairiukstis*, 1990]. Standard (detrended) ring-width values were not normalized, in order to preserve the effect of the relative contribution of trees of different diameters to overall productivity. The effect of the additional processing was minimal. There was no trend evident in the mean ring widths based on raw widths or in the means based on "detrended" widths (P=0.334; P=0.559). Patterns of year-to-year variation and correlation with NPP estimates were similar (Table 4).

Appendix C

Correction for Volcanic Aerosols Applied to "PRE" and FASIR NDVI Versions

This correction [*Sellers et al.*, 1996; S.O. Los, manuscript in preparation, 1997] was applied to the 1982-1984 global NDVI data to account for the effects of aerosols produced by the eruption of El Chichón (Chiapas, Mexico) in April 1982. A relationship was derived between the optical thickness data of *Vermote et al.* [1994], obtained over the Pacific Ocean, and deviations in the NDVI values over the land surface. It was

assumed that the aerosol optical thickness was constant with longitude and varied only with latitude and time since eruption. Because of the high mixing rates and strong longitudinal component of wind in the upper atmosphere, this assumption is reasonable for the period beginning a few months after the initial eruption but may not be so for the first months.

The deviation in NDVI values was estimated by latitudinal band for May 1982 through December 1984 from regions with mean monthly NDVI greater than 0.5. Because regions with high mean NDVI values generally exhibit low temporal variation [*Tucker et al.*, 1985; S.O. Los, manuscript in preparation, 1997], it was assumed that deviation in NDVI in these regions was caused primarily by El Chichón aerosols. A relationship between deviation in NDVI and the optical thickness data was then determined (S.O. Los, manuscript in preparation, 1997), assuming that deviation in NDVI varied linearly with NDVI [*Vermote et al.*, 1994]. The global NDVI data were then adjusted on the basis of estimates of optical thickness, as a function of latitude and time.

Solar Zenith Angle Correction Applied to the FASIR NDVI Version

The effect of solar zenith angle (SZA) on the global NDVI data was estimated from a statistical analysis of NDVI distributions. The SZA effect was established for two situations where interannual variation in NDVI is low: bare soils and land cover types with dense vegetation [*Sellers et al.*, 1996; S.O. Los, manuscript in preparation, 1997]. The analysis of solar zenith angle on dense vegetation was restricted to land cover types with tall vegetation (SiB classes 1 through 6) and agriculture (SiB class 12). The monthly NDVI data for 1982-1990 were stratified by vegetation type and solar zenith angle (S.O. Los, manuscript in preparation, 1997). For example, data from a deciduous forest at 50°N for July were merged with data from a deciduous forest at 20°S for January (the bias in latitude is caused by the overpass time of the satellite). The analysis was further restricted to areas with noon solar zenith angles smaller than 35° to avoid using data from dormant vegetation. NDVI frequency distributions were calculated for each of the stratified sets of data. The 98th percentiles of these distributions were assumed to correspond to fully green conditions. For each vegetation class, the 98th percentiles were plotted against solar zenith angle. The 98th percentile values show an exponential decrease in NDVI with increasing solar zenith angle. The analysis was repeated for NDVI populations from bare soils and deserts (SiB classes 9 and 11) using the 2nd percentiles instead of the 98th. No significant effect of solar zenith angle on the NDVI of bare areas was found. A similar conclusion was drawn by *Los* [1997] from an analysis of sensor degradation effects over desert areas. This conclusion is somewhat at odds with the earlier study of Sellers *et al.* [1996] in which, based on the analysis of one year of data, a small solar zenith angle effect was found in NDVI values from deserts. With the solar zenith angle effect estimated for the two extremes, intermediate values were corrected assuming a linear effect of solar zenith angle with NDVI. The NDVI values for the entire data record were restored to values corresponding to a solar zenith angle of 30°.

Appendix D: Notes on Other Models

The Frankfurt Biosphere Model (FBM) is a climate-driven model that predicts phenology and calculates NPP as a function of photosynthetic uptake and autotrophic respiration [*Lüdecke et al.*, 1994; *Kindermann et al.*, 1993]. In *Kindermann et al.*'s [1996] multiyear study, FBM was driven with temperature anomalies based on measurements by the microwave sounding units on both the morning and afternoon NOAA satellites [*Christy and Drouilhet*, 1994], which were added to the *Leemans and Cramer* [1991] mean set. Precipitation was derived by adding the *Baker et al.* [1995] anomalies to the Leemans and Cramer means.

The *Maisongrande et al.* [1995] model also calculates NPP as a function of photosynthetic uptake and autotrophic respiration, but like CASA takes a light-use efficiency approach that relies on NDVI-based estimates of FPAR, as well as on temperature [*Leemans and Cramer*, 1991] and solar radiation [*Planton et al.*, 1991] input sets. Unlike CASA, FBM, and the Miami model, the Maisongrande et al. model does not use precipitation data. The multiyear estimates published by *Maisongrande et al.* [1995] were based on variable NDVI but on mean temperature and solar radiation.

Acknowledgments. We thank Anne Ruimy for the CESBIO NDVI version, Dan Baldwin (Colorado State University) for the original equatorial crossing time program, F.-W. Badeck for the global FBM estimates, and Jasmin John for help with the meteorological data. We also thank the Distributed Active Archive Center (Code 902.2) at the Goddard Space Flight Center, Greenbelt, Maryland, for producing the Pathfinder data and distributing them. The original Pathfinder data products were produced under the NOAA/NASA Pathfinder program, by a processing team headed by Mary James of the Goddard Global Change Data Center; and the science algorithms were established by the AVHRR Land Sciences Working Group, chaired by John Townshend of the University of Maryland. Goddard's contributions to these activities were sponsored by NASA's Mission to Planet Earth Program. We also wish to thank the helpful staffs at the Canadian Wheat Board, Statistics Canada, the USDA-NASS and Departments of Agriculture in Kansas and Oklahoma, the USDA Foreign Agricultural Service, and the Grains Research and Development Corporation in Australia, and N. M. Holbrook. Burt Bartlett at the Oklahoma Department of Agriculture, Katherine Chambers, reference librarian at the University of California, Davis, Emily Binnian, USGS, and Andrew Weiss, Center for Conservation Biology, were particularly helpful. We appreciate the critical comments of Franz-W. Badeck, Deborah Gordon, Anne Ruimy, Peter Vitousek, and three anonymous reviewers, and the support of the WESTGEC component of the DOE NIGEC program and the NASA EOS-IDS program. C. Malmström was supported by a U.S. Department of Energy Graduate Fellowship for Global Change (administered by the Oak Ridge Institute for Science and Education), G. Juday was supported by NSF grant DEB 9211769 for the Bonanza Creek Long-Term Ecological Research Site and by the USDA MacIntire-Stennis Cooperative Forestry Research Program, J. Randerson was supported by a NASA Global Change Fellowship, and S. Los was supported by a NASA EOS-IDS grant (Sellers-Randall-Mooney), contract NAS5-31732. This is Carnegie Institution of Washington publication number 1330.

References

Agbu, P.A., and M.E. James, *The NOAA/Pathfinder AVHRR Land Data Set User's Manual*, Goddard Distrib. Active Arch. Cent., NASA Goddard Space Flight Cent., Greenbelt, Md., 1994.

Australian Bureau of Statistics, *Year Book Australia*, Canberra, A.C.T, 1990.

Australian Bureau of Statistics, *Year Book Australia*, Canberra, A.C.T, 1994.

Baker, C.B., J.K. Eischeid, T.R. Karl, and H.F. Diaz, The quality control of long-term climatological data using objective data analysis, paper presented at Ninth Conference on Applied Climatology, Am. Meteorol. Soc., Dallas, Tex., Jan. 15-20, 1995.

Bishop, J.K.B., and W.B. Rossow, Spatial and temporal variability of global surface solar irradiance, *J. Geophys. Res., 96,* 16839-16858, 1991.

Briffa, K.R., P.D. Jones, F.H. Schweingruber, S.G. Shiyatov, and E.R. Cook, Unusual twentieth-century summer warmth in a 1000-year temperature record from Siberia, *Nature, 376,* 156-159, 1995.

Canadian Wheat Board, Weather and Crop Surveillance Department, *Permit Book Acreage Maps*, Winnipeg, Manit., Canada, 1989.

Canadian Wheat Board, Weather and Crop Surveillance Department, *Permit Book Acreage Maps*, Winnipeg, Manit., Canada, 1994.

Central Intelligence Agency (CIA), *The World Factbook 1995,* U.S. Govt. Print. Off., Washington, D. C., 1995.

Christy, J.R., and S.J. Drouilhet, Variations in daily, zonal mean lower stratospheric temperatures, *J. of Clim., 7,* 106-120, 1994.

Comeau, A., and G. Barnett, Effect of barley yellow dwarf virus on N, P, K fertilizer efficiency and on the harvest index of oats, *Can. J. Plant Sci., 59,* 43-54, 1979.

Cook, E.R., A time series analysis approach to tree-ring standardization, Ph.D. thesis, Univ. of Ariz., Tucson, 1985.

Cook, E.R., and L.A. Kairiukstis, *Methods of Dendrochronology,* Kluwer Acad., Norwell, Mass., 1990.

Dai, A., and I. Y. Fung, Can climate variability contribute to the "missing" carbon dioxide sink?, *Global Biogeochem. Cycles, 7*(3), 599-609, 1993.

Davidson, J. L., and J.W. Birch, Responses of a standard Australian and a Mexican wheat to temperature and water stress, *Austr. J. Agric. Res. 29,* 1091-1106, 1978.

Deering, D.W., and T.F. Eck, Atmospheric optical depth effects on angular anisotropy of plant canopy reflectance, *Int. J. Remote Sens., 8,* 89-916, 1987.

Deering, D.W., E.M. Middleton, J.R. Irons, B.L. Blad, E.A. Walter-Shea, C.J. Hayes, C.W. Walthall, T.F. Eck, S.P. Ahmad, and B.P. Banerjee, Prairie grassland bi-directional reflectance measured by different instruments at the FIFE sites, *J. Geophys. Res. 97,* 18887-18903, 1992a.

Deering, D.W., T.F. Eck, and T. Grier, Shinnery oak bidirectional reflectance properties and canopy model inversion, *IEEE Trans. Geosci. Remote Sens. 30,* 339-348, 1992b.

DeFries, R.S., and J.R.G. Townshend, NDVI-derived land cover classification at a global scale, *Int. J. Remote Sens., 15,* 3567-3586, 1994.

DeFries, R.S., and J.R.G. Townshend, An initial coarse resolution NDVI-derived global land cover classification, in *International Satellite Land Surface Climatology Project Initiative I--Global Data Sets for Land-Atmosphere Models, 1987-1988,* vols. 1-5, edited by B. W. Meeson et al., [CD-ROM USA_NASA-GDAAC_ISLSCP_001 - USA_NASA_GDAAC_ISLSCP_005], Goddard Distrib. Active Arch. Cent., NASA Goddard Space Flight Cent., Greenbelt, Md., 1995.

Devlet Istatistik Enstitusu, *Turkiye Istatistik Yilligi*, Ankara, Turkey, 1987.

Devlet Istatistik Enstitusu, *Turkiye Istatistik Yilligi*, Ankara, Turkey, 1993.

Farquhar, G.D., S. von Caemmerer, and J.A. Berry, A biochemical model of photosynthetic CO_2 assimilation in leaves of C3 species, *Planta, 149,* 79-90, 1980.

Field, C.B., J.T. Randerson, and C.M. Malmström, Global net primary production: Combining ecology and remote sensing, *Remote Sens. Environ. 51,* 74-88, 1995.

Food and Agriculture Organization of the United Nations, *FAO Production Yearbook*, Rome, 1984.

Food and Agriculture Organization of the United Nations, *FAO Production Yearbook*, Rome, 1986.

Food and Agriculture Organization of the United Nations, *FAO Production Yearbook*, Rome, 1989.

Food and Agriculture Organization of the United Nations, *FAO Production Yearbook*, Rome, 1990.

Francey, R.J., P.P. Tans, C.E. Allison, I.G. Enting, J.W.C. White, and M. Trolier, Changes in oceanic and terrestrial carbon uptake since 1982, *Nature, 373,* 326-330, 1995.

Friedlingstein, P., I. Fung, E. Holland, J. John, G. Brasseur, D. Erickson, and D. Schimel, On the contribution of CO_2 fertilization to the missing biospheric sink, *Global Biogeochem. Cycles, 9*(4), 541-556, 1995.

Fritts, H.C., *Tree Rings and Climate*, Academic, San Diego, Calif., 1976.

Goward, S.N., B. Markham, D.G. Dye, W. Dulaney, and J. Yang, Normalized difference vegetation index measurements from the advanced very high resolution radiometer, *Remote Sens. Environ., 35,* 257-277, 1991.

Goward, S.N., S. Turner, D.G. Dye, and S. Liang, The University of Maryland improved Global Vegetation Index product, *Int. J. Remote Sens. 15,* 3365-3395, 1994.

Gutman, G.G., Vegetation indices from AVHRR: An update and future prospects, *Remote Sens. Environ., 35,* 121-136, 1991.

Hansen, J., and S. Lebedeff, Global trends of measured surface air temperature, *J. Geophys. Res., 92,* 13345-13372, 1987.

Hansen, J., and S. Lebedeff, Global surface air temperatures: Update through 1987, *Geophys. Res. Lett. 15,* 323-326, 1988.

Hay, R.K.M., Harvest index: A review of its use in breeding and crop physiology, *Ann. of Appl. Biol., 126,* 197-216, 1995.

Holben, B.N., Characteristics of maximum-value composite images from temporal AVHRR data, *Int. J. Remote Sens., 7,* 1417-1434, 1986.

Houghton, R.A., Changes in terrestrial carbon over the last 135 years, in *The Global Carbon Cycle,* edited by M. Heimann, pp. 139-157, Springer-Verlag, New York, 1993.

Hucl, P., and R.J. Baker, A study of ancestral and modern Canadian spring wheats, *Can. J. Plant Sci. 67,* 87-97, 1987.

Jacoby, G.C., and R.D. D'Arrigo, Reconstructed northern hemisphere annual temperature since 1671 based on high-latitude tree-ring data from North America, *Clim. Change, 14*(1), 39-60, 1989.

Jacoby, G. C., and R.D. D'Arrigo, Tree ring width and density evidence of climatic and potential forest change in Alaska, *Global Biogeochem.Cycles, 9*(2), 227-234, 1995.

James, M.E., and S.N.V. Kalluri, The Pathfinder AVHRR land data set: An improved coarse resolution data set for terrestrial monitoring, *Int. J. Remote Sens., 15,* 3347-3363, 1994.

Justice, C.O., T.F. Eck, D. Tanré, and B.N. Holben, The effect of water vapor on the normalized difference vegetation index for the Sahelian region from NOAA-AVHRR data, *Int. J. Remote Sens., 12,* 1165-1187, 1991.

Kansas Department of Agriculture, Division of Statistics, Wheat acreage, yield, and production by county, Topeka, Kansas, 1985.

Kaufman, Y.J., and B.N. Holben, Calibration of the AVHRR visible and near-IR bands by atmospheric scattering, ocean glint, and desert reflection, *Int. J. Remote Sens., 14,* 21-52, 1993.

Keeling, C.D., and T.P. Whorf, Atmospheric CO_2--Modern record: Mauna Loa, in *Trends 91: A Compendium of Data on Global Change,* edited by T. A. Boden et al., Carbon Dioxide Information Analysis Center, Oak Ridge, Tenn., 1991.

Keeling, C.D., T.P. Whorf, M. Whalen, and J. van der Plicht, Interannual extremes in the rate of rise of atmospheric carbon dioxide since 1980, *Nature, 375,* 666-670, 1995.

Kindermann, J., et al., Structure of a global carbon exchange model for the terrestrial biosphere: The Frankfurt Biosphere Model (FBM), *Water Air Soil Pollut., 70,* 675-684, 1993.

Kindermann, J., F.-W. Badeck, G. Würth, and G. H. Kohlmaier, Interannual variation of carbon exchange fluxes in terrestrial ecosystems, *Global Biogeochem. Cycles, 10*(4), *737-755*, 1996.

Lau, K.-M., and P.J. Sheu, Teleconnections in global rainfall anomalies: Seasonal to inter-decadal time scales, in *Teleconnections Linking Worldwide Climate Anomalies,* edited by M. H. Glantz et al., pp. 227-256, Cambridge Univ. Press, New York, 1991.

Lazenby, A., M. Bartholomaeus, B. Boucher, W.R. Boyd, A. Campbell, R. Cracknell, H. Eagles, J. Lee, G. Lukey, and B. Marshall, *Trials and Errors: A Review of Variety Testing and Release Procedures in the Australian Grains Industry*, Grains Res. and Dev. Corp., Canberra, A.C.T., 1994.

Leemans, R., and W.P.Cramer, The IIASA database for mean monthly values of temperature, precipitation and cloudiness of a global terrestrial grid, *Res. Rep. RR-91-18,* Int. Inst. of Appl. Syst. Analy., Laxenburg, Austria, 1991.

Lieth, H., Modeling the primary productivity of the world, in *Primary Productivity of the Biosphere,* edited by H. Lieth and R. H. Whittaker, pp. 237-263, Springer-Verlag, New York, 1975.

Los, S.O., Calibration adjustment of the NOAA AVHRR normalized difference vegetation index without recourse to component channel 1 and 2 data, *Int. J. Remote Sens., 14,* 1907-1917, 1993.

Los, S.O., Estimation of the ratio of sensor degradation between NOAA-AVHRR channels 1 and 2 from monthly NDVI composites, *IEEE Trans. Geosci. Remote Sens.,* in press, 1997.

Los, S.O., C.O. Justice, and C.J. Tucker, A global 1° by 1° NDVI data set for climate studies derived from the GIMMs continental NDVI data, *Int. J. Remote Sens., 15,* 3493-3518, 1994.

Lüdecke, M., et al., The Frankfurt Biosphere Model: A global process oriented model for the seasonal and long-term CO_2 exchange between terrestrial ecosystems and the atmosphere, *Clim. Res., 4*(2), 143-166, 1994.

Luo, Y., and H.A. Mooney, Stimulation of global photosynthetic carbon influx by an increase in atmospheric carbon dioxide concentration, in *Carbon Dioxide and Terrestrial Ecosystems*, edited by G. W. Koch and H. A. Mooney, pp. 381-397, Academic, San Diego, Calif., 1996.

Maisongrande, P., A. Ruimy, G. Dedieu, and B. Saugier, Monitoring seasonal and interannual variations in gross primary productivity, net primary productivity and net ecosystem productivity using a diagnostic model and remotely-sensed data, *Tellus, Ser. B, 47,* 178-190, 1995.

Malmström, C.M., J.T. Randerson, M.V. Thompson, H.A. Mooney, and C.B. Field, The next dimension: Extending the time axis of global NPP estimates, in *Proceedings of the International Colloquium Photosynthesis and Remote Sensing, 28-30 August 1995, Montpellier, France,* edited by G. Guyot, pp. 407-411, Eur. Assoc. of Remote Sens. Lab., Paris, and Institut National de la Recherche Agronomique, Avignon, France, 1995.

Mattern, P.J., Wheat, in *Handbook of Cereal Science and Technology*, edited by K. J. Lorenz and K. Cult, pp. 1-54, Marcel Dekker, New York, 1991.

Monteith, J.L., Solar radiation and productivity in tropical ecosystems, *J. Appl. Ecol., 9,* 747-766, 1972.

Monteith, J.L., Climate and the efficiency of crop production in Britain, *Philos. Trans. R. Soc. London Ser. B., 281,* 277-294, 1977.

Myneni, R.B., S.O. Los, and G. Asrar, Potential gross primary productivity of terrestrial vegetation from 1982-1990, *Geophys. Res. Lett., 22*(19), 2617-2620, 1995.

Myneni, R.B., C.D. Keeling, C.J. Tucker, G. Asrar, and R.R. Nemani, Increased plant growth in the northern high latitudes from 1981 to 1991, *Nature, 386,* 698-702, 1997.

Nobel, P. S. *Physicochemical and Environmental Plant Physiology*, Academic, San Diego, Calif., 1991.

Oklahoma Department of Agriculture, Oklahoma Agricultural Statistics Service, Oklahoma crop production: 1987 crop review, Oklahoma City, Okla., 1987a.

Oklahoma Department of Agriculture, Oklahoma Agricultural Statistics Service, Oklahoma crop-weather summary: 1987 crop weather review, Oklahoma City, Okla., 1987b.

Oklahoma Department of Agriculture, Oklahoma Agricultural Statistics Service, 1996 Oklahoma winter wheat, cotton, and sorghum estimates by county, Oklahoma City, Okla., 1987c.

Passioura, J.B., Grain yield, harvest index, and water use of wheat, *J. Aust. Inst. Agric. Sci.,* Sept/Dec, 117-120, 1977.

Perry, M.W., Cereal and fallow/pasture systems in Australia, in *Field Crop Ecosystems*, edited by C. J. Pearson, pp. 451-483, Elsevier, New York, 1992.

Planton, S., M. Déqué, and C. Bellevaux, Validation of an annual cycle simulation with a T42-L20 GCM, *Clim. Dyn., 5,* 189-200, 1991.

Potter, C.S., J.T. Randerson, C.B. Field, P.A. Matson, P.M. Vitousek, H.A. Mooney, and S.A. Klooster, Terrestrial ecosystem production: A process model based on global satellite and surface data, *Global Biogeochem. Cycles, 7,* 811-841, 1993.

Price, J.C., Timing of NOAA afternoon passes, *Int. J. Remote Sens., 12(1),* 193-198, 1991.

Privette, J.L., C. Fowler, G.A. Wick, D. Baldwin, and W.J. Emery, Effects of orbital drift on advanced very high resolution radiometer products: normalized difference vegetation index and sea surface temperature, *Remote Sens. Environ. 53,* 164-171, 1995.

Raich, J.W., E.B. Rastetter, J.M. Melillo, D.W. Kicklighter, P.A. Steudler, B.J. Peterson, A.L. Grace, B.I. Moore, and C.J. Vorosmarty, Potential net primary productivity in South America: Application of a global model, *Ecol. Appl. 1*(4), 399-429, 1991.

Randerson, J.T., M.V. Thompson, C.M. Malmström, C.B. Field, and I.Y. Fung, Substrate limitations for heterotrophs: Implications for models that estimate the seasonal cycle of atmospheric CO_2, *Global Biogeochem. Cycles, 10*(4), 585-602, 1996.

Rao, C.R.N., Non-linearity corrections for the thermal infrared channels of the advanced very high resolution radiometer: Assessment and recommendations. *NOAA Tech. Rep. NESDIS-69,* Natl. Oceanic and Atmos. Admin., Natl. Environ. Satell. Data and Inf. Serv., Washington, D. C., 1993a.

Rao, C.R.N., Degradation of the visible and near-infrared channels of the advanced very high resolution radiometer on the NOAA-9 spacecraft: Assessment and recommendations for corrections. *NOAA Tech. Rep. NESDIS-70,* Natl. Oceanic and Atmos. Admin., Natl. Environ. Satell. Data and Inf. Serv., Washington, D. C., 1993b.

Rao, C.R.N., and J. Chen, Inter-satellite calibration linkages for the visible and near-infrared channels of the advanced very high resolution radiometer on the NOAA-7, -9, and -11 spacecraft, *Int. J. Remote Sens., 16,* 1931-1942, 1995.

Rasmusson, E.M., Observational aspects of ENSO cycle teleconnections, in *Teleconnections Linking Worldwide Climate Anomalies,* edited by M. H. Glantz et al., pp. 309-344, Cambridge Univ. Press, New York, 1991.

Rosborough, G.W., D.G. Baldwin, and W.J. Emery, Precise AVHRR image navigation, *IEEE Trans. Geosci. Remote Sens., 32,* 644-657, 1994.

Ruimy, A., B. Saugier, and G. Dedieu, Methodology for the estimation of terrestrial net primary production from remotely sensed data, *J. Geophys. Res., 99,* 5263-5283, 1994.

Sarmiento, J.L., C. Le Quéré, and S.W. Pacala, Limiting future atmospheric carbon dioxide, *Global Biogeochem. Cycles, 9,* 121-137, 1995.

Schimel, D.S., I.G. Enting, M. Heimann, T.M.L. Wigley, D. Raynaud, D. Alves, and U. Siegenthaler, CO_2 and the carbon cycle, in *Climate Change 1994: Radiative Forcing of Climate Change and an Evaluation of IPCC IS92 Emission Scenarios,* edited by J. T. Houghton, et al., pp. 35-71, Cambridge Univ. Press, New York, 1995.

Schlesinger, W.H., *Biogeochemistry: An Analysis of Global Change*, Academic, San Diego, Calif., 1991.

Sellers, P.J., J.A. Berry, G.J. Collatz, C.B. Field, and F.G. Hall, Canopy reflectance, photosynthesis, and transpiration, III, Reanalysis using improved leaf models and a new canopy integration scheme, *Remote Sens. Environ., 42*(3), 187-216, 1992.

Sellers, P.J., S.O. Los, C.J. Tucker, C.O. Justice, D.A. Dazlich, G. J. Collatz, and D.A. Randall, A revised land surface parameterization (SiB2) for atmospheric GCMs, II, The generation of global fields of terrestrial biophysical parameters from satellite data. *J. Clim., 9*(4), 706-737, 1996.

Shea, D.J., Climatological atlas: 1950-1979, *Tech. Note NCAR TN-269+STR,* Natl. Cent. for Atmos. Res., Boulder, Colo., 1986.

Siddique, K.H.M., R. K. Belford, M.W. Perry, and D. Tennant, Growth, development and light interception of old and modern wheat cultivars in a mediterranean-type environment, *Aust. J. Agric. Res., 40,* 473-487, 1989.

Siddique, K.H.M., R.K. Belford, and D. Tennant, Root:shoot ratios of old and modern, tall and semi-dwarf wheats in a mediterranean environment, *Plant Soil, 121,* 89-98, 1990.

Singh, S.M., Simulation of solar zenith angle effect on global vegetation index (GVI) data, *Int. J. Remote Sens., 9,* 237-248, 1988a.

Singh, S.M., Lowest order correction for solar zenith angle to global vegetation index (GVI) data, *Int. J. Remote Sens., 9,* 1565-1572, 1988b.

Smika, D.E., Cereal systems of the North American Central Great Plains, in *Field Crop Ecosystems,* edited by C. J. Pearson, pp. 401-412, Elsevier, New York, 1992.

Sokal, R.R., and F. J. Rohlf, *Biometry, 2nd ed.,* W. H. Freeman, New York, 1981.

Statistics Canada, *Canada Year Book,* Ottawa, Ont., 1985.

Statistics Canada, *Field Crop Reporting Series*, Catalog No. 22002 EXPB, Ottawa, Ont., 1987.

Statistics Canada,*Canada Year Book*, Ottawa, Ont., 1988a.

Statistics Canada, *Field Crop Reporting Series*, Catalog No. 22002 EXPB, Ottawa, Ont., 1988b.

Statistics Canada, *Field Crop Reporting Series*, Catalog No. 22002 EXPB, Ottawa, Ont., 1989.

Statistics Canada, *Field Crop Reporting Series*, Catalog No. 22002 EXPB, Ottawa, Ont., 1990.

Statistics Canada, *Agricultural Census*, Ottawa, Ont., 1991.

Tarpley, J.D., S.R. Schneider, and R.L. Money, Global vegetation indices from the NOAA-7 meteorological satellite, *J. Clim. Appl. Meteorol., 23*, 491-494, 1984.

Thompson, M.V., J.T. Randerson, C.M. Malmström, and C.B. Field, Change in net primary production and heterotrophic respiration: How much is necessary to sustain the terrestrial carbon sink?, *Global Biogeochem. Cycles, 10*(4), 711-726, 1996.

Townshend, J.R.G., Global data sets for land applications from the advanced very high resolution radiometer: An introduction, *Int. J. Remote Sens., 15*, 3319-3332, 1994.

Trenberth, K.E., General characteristics of El Niño-Southern Oscillation, in *Teleconnections Linking Worldwide Climate Anomalies*, edited by M. H. Glantz et al., pp. 13-42, Cambridge Univ. Press, New York, 1991.

Trenberth, K.E., G. W. Branstator, and P.A. Arkin, Origins of the 1988 North American drought, *Science, 242*, 1640-1645, 1988.

Tucker, C.J., J.R.G. Townshend, and T.E. Goff, African land-cover classification using satellite data, *Science, 227*, 369-375, 1985.

U.S. Department of Agriculture, Foreign Agricultural Service, Foreign agriculture 1990-1991, Washington, D. C., 1991.

U.S. Department of Agriculture, National Agricultural Statistics Service, Agricultural statistics, U.S. Govt. Print. Off., Washington, D. C., 1993.

U.S. Department of Agriculture, National Agricultural Statistics Service, Kansas agricultural statistics: Wheat, corn, sorghum and soybean irrigated acres by county, Topeka, Kans., 1995.

U.S. Department of Agriculture, National Agricultural Statistics Service, Kansas agricultural statistics: 1996 Kansas farm facts, Topeka, Kansas, 1996.

U.S. Department of Agriculture, World Agricultural Outlook Board, Major world crop areas and climatic profiles, U.S. Govt. Print. Off., Washington, D. C., 1994.

U.S. Department of Commerce, Statistical abstract of the United States, U.S. Govt. Print. Off., Washington, D. C., 1984.

U.S. Department of Commerce, Statistical abstract of the United States, U.S. Govt. Print. Off., Washington, D. C., 1985.

U.S. Department of Commerce, Statistical abstract of the United States, U.S. Govt. Print. Off., Washington, D. C., 1987.

U.S. Department of Commerce, Statistical abstract of the United States, U.S. Govt. Print. Off., Washington, D. C., 1989.

U.S. Department of Commerce, Statistical abstract of the United States, U.S. Govt. Print. Off., Washington, D. C., 1991.

U.S. Department of Commerce, Statistical abstract of the United States, U.S. Govt. Print. Off., Washington, D. C., 1992.

U.S. Geological Survey, Alaska land characteristics data set--Interim statewide landcover classification, Eros Data Cent. and Eros Alaska Field Off., Natl. Mapp. Div., Anchorage, Alaska, 1994.

Van Royen, W., *The Atlas of the World's Resources*, volume 1, *The Agricultural Resources of the World*, Prentice-Hall, Englewood Cliffs, N.J., 1952.

Vermote, E.F., N. El Saleous, Y.J. Kaufman, and E. Dutton, Data preprocessing: Stratospheric aerosol perturbing effect on the remote sensing of vegetation: Correction method for the composite NDVI after the Pinatubo eruption, paper presented at Société Internationale de Photogrammé et de Télédétection (ISPRS) Sixième Symposium. Internationale, Val d'Isere, France, 1994.

Walker, G.W., Weather sensitivity of western Canada wheat yield, 1900-1988, *Can. J. Soil Sci., 69*, 857-865, 1989.

Woodhead, T., R. Huke, E. Huke, and L. Balababa, *Rice-Wheat Atlas of India*, Int. Rice Res. Inst., Manila, Philippines, 1994.

Zobler, L.A., World soil file for global climate modeling, *NASA Tech. Memo., 87802*, 32 pp., 1986.

C. B. Field and J. T. Randerson, Carnegie Institution of Washington, Department of Plant Biology, 290 Panama St., Stanford, CA 94305-1297. (e-mail: chris@jasper.stanford.edu; orcinus@jasper.stanford.edu)

G. P. Juday, Forest Sciences Department, University of Alaska-Fairbanks, P.O. Box 757200, Fairbanks, AK 99775. (e-mail: gjuday@gis.lter.alaska.edu)

S. O. Los, NASA Goddard Space Flight Center, Code 923, Greenbelt, MD 20771. (e-mail: sietse@scirocco.gsfc.nasa.gov)

C. M. Malmström (corresponding author), Department of Integrative Biology, University of California, Berkeley, Berkeley, CA 94720. (e-mail: malmstrm@socrates.berkeley.edu)

M. V. Thompson, Department of Organismic and Evolutionary Biology, Harvard University, 16 Divinity Avenue, Cambridge, MA 02138. (e-mail: mthompso@oeb.harvard.edu)

(Received November 27, 1996; revised May 5, 1997;
accepted May 12, 1997.)